Extensional tectonic origin of gneissosity and related structures of the Feiran–Solaf metamorphic belt, Sinai, Egypt

A. Fowler [a,*], I. Hassan [b]

[a] *Geology Department, United Arab Emirates University, Faculty of Science, P.O. Box 17551, Al-Ain, United Arab Emirates*
[b] *Geology Department, Suez Canal University, Ismailia, Egypt*

ARTICLE INFO

ABSTRACT

The Feiran–Solaf metamorphic belt consists of low-P high-T amphibolite facies, partly migmatized gneisses, schists, amphibolites and minor calc-silicate rocks of metasedimentary origin. There are also thick concordant synkinematic sheets of diorite, tonalite and granodiorite orthogneiss and foliated granite and pegmatite dykelets. The gneissosity (or schistosity) is referred to as S_1, and is almost everywhere parallel to lithological layering, S_0. This parallelism is not due to transposition. The gneissosity formed during an extensional tectonic event (termed D1), before folding of S_0. S_1 formed by coaxial pure shear flattening strain (Z normal to S_0, i.e. vertical; with X and Y both extensional and lying in S_1). This strain also produced chocolate tablet boudinage of some layers and S_1-concordant sills and veins. S_1 has a strong stretching lineation L_1 with rodding characteristics. Within-plane plastic anisotropy (lower ductility along Y compared to along X) resulted in L_1-parallel extensional ductile shears and melt filled cracks. Continued shortening of these veins, and back-rotation of foliations on the shears produced intrafolial F_1 folds with hinges parallel to the stretching lineation. F_1 fold asymmetry variations do not support previous models involving macroscopic F_1 folds or syn-gneissosity compressional tectonics. The sedimentary protoliths of the Feiran–Solaf gneisses were probably deposited in a pre-800 Ma actively extending intracratonic rift characterizing an early stage of the break-up of Rodinia.

© 2008 Elsevier B.V. All rights reserved.

1. Introduction

There have been many petrological studies of the migmatites, gneisses and amphibolites that form a narrow NW-SE trending belt along wadis Feiran and Solaf in the western Sinai (Akaad, 1959; Akaad et al., 1967a; El-Gaby and Ahmed, 1980; Ahmed, 1981; Soliman et al., 1988; El Tokhi, 1990; Belasy, 1991; Hashad et al., 2001) (Fig. 1). However, the shortage of structural studies of the same rocks (Hegazi, 1988; Abdel-Meguid, 1992; El-Shafei, 1998; El-Shafei and Kusky, 2003; Hegazi et al., 2004) is a major obstacle to understanding the significance of the gneissic rocks of the Sinai and Egyptian Eastern Desert. The aim of this contribution is to offer some additional structural observations and alternative views on the origin of the gneissosity and related structures of the Feiran–Solaf belt, and especially to investigate the tectonic environment in which the gneisses formed. Post-gneissosity structures are the subject of a separate contribution in preparation, and will only be briefly mentioned in this paper.

The Feiran–Solaf gneisses form a NW-trending 40 km × 8 km strip of rocks dissected by the NW-draining Wadi Feiran and Wadi Solaf on the southwestern side of the Sinai Peninsula (Fig. 1). The main tributary wadis of this area referred to in the text are also shown in Fig. 1.

2. Previous work

The first observations on the Sinai gneissic rocks were those of Hume (1906), Barron (1907) and Ball (1916), with detailed reports on the Feiran–Solaf metamorphics provided by Hume (1934), who considered the gneisses to represent very old continental crust. Schürmann (1953, 1966) compared the Feiran gneisses with other gneissic rocks of the Eastern Desert and pictured the orthogneisses and migmatites as basement rocks. These studies identified the common lithologies of the Feiran–Solaf metamorphics as biotite- and hornblende-bearing gneiss, quartzo-feldspathic gneiss, amphibolite, biotite schist, calc-silicate gneiss and abundant pegmatite.

2.1. Migmatization studies

Early detailed work on the Feiran–Solaf gneisses concentrated on identifying the protolith, metamorphic facies and petrological

---
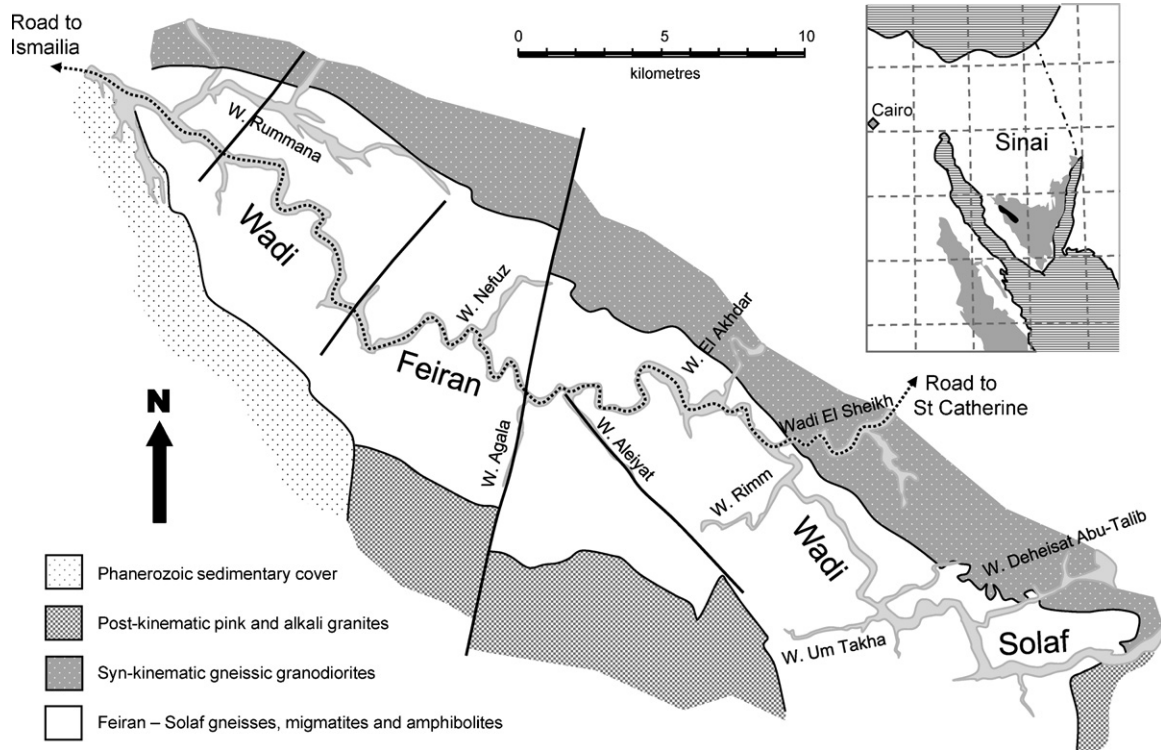
Fig. 1. Locality map for the Wadi Feiran—Wadi Solaf area in the SW of Sinai. The names of the main tributary wadis mentioned in the text are also shown. Dark lines on the Feiran–Solaf map are faults (e.g. along Wadis Agala and Aleiyat). Dotted line represents the sealed road along the main wadi.

evolution of these rocks (Akaad, 1959; El-Gaby, 1967; Akaad et al., 1967a). These contributions were consolidated in Akaad et al. (1967b) who concluded that (1) the gneissic rocks were mainly geosynclinal pelitic, psammitic and carbonate metasediments, though some amphibolites may have been sills or flows, (2) the metamorphic grade did not exceed amphibolite facies, and (3) the rocks were first regionally metamorphosed, then temperatures rose and partial melting (anatexis) began in rocks with sufficiently high P_{H_2O}.

2.2. Stratigraphic approach and discovery of the main macrofolds

Comprehensive mapping of the gneissic rocks by Ahmed (1970) added a stratigraphic and basic structural framework to the earlier mainly petrological studies. The metasedimentary gneisses were collected into lithostratigraphic units with formation and member status. These were reorganized by El-Gaby and Ahmed (1980) into two subgroups (Feiran and Solaf), five formations and ten members. The stratigraphic units were based on lithological distinctions that could be traced for distances of up to 20 km. More recently, lithological map units have been preferred (e.g. El-Shafei and Kusky, 2003, and this study—see Fig. 2). El-Gaby and Ahmed's (1980) stratigraphic approach yielded two important results. The first is that the formations acted as marker horizons to reveal two doubly plunging macroscopic antiforms with WNW to NW trend (the Feiran and Solaf anticlines). The second was that temperature-dependent effects, e.g. migmatization and metamorphic grade were shown to increase stratigraphically downwards, being highest in the deepest unit, the Nidia El-Samra Fm. Lower metamorphic grade in higher stratigraphic units was also reported by Ahmed (1981). The absence of any evidence for regional scale stratigraphic repetition indicated that the high

grade metamorphism occurred before significant folding of the units.

2.3. Determining metamorphic P–T conditions

Ahmed (1981) noted that while a sillimanite-muscovite zone was present, a staurolite-kyanite zone was not. He concluded that the pressures of metamorphism were too low for kyanite. Studies of the migmatization process (El Tokhi, 1990) and amphibolite phase assemblages (El Tokhi, 1992) confirm the low pressure–high temperature amphibolite facies regional metamorphism responsible for gneissification of the rocks. El Tokhi (1990) estimated $P < 5$ kbar and $T \sim 640$ to $700\,°C$ at the time of anatexis. El Tokhi (1992) calculated a pressure of 2–4 kbar and $T \sim 550$ to $740\,°C$ for the metamorphism of the amphibolites. Eliwa et al. (2004) estimated $T \sim 638$ to $677\,°C$ and P of 4–5 kbar for the Solaf zone biotite-hornblende gneisses.

2.4. Deformation events and their relations to metamorphism

The deformation events and relations between mesoscopic structures, macroscopic structures and metamorphism were investigated by Hegazi (1988), Belasy (1991), Kabesh (1993), El-Shafei (1998) and Sultan (2003). Hegazi (1988) discovered that the gneisses had two phases of deformation D1 and D2 accompanied by two high temperature metamorphic events M1 and M2. He concluded that there were three significant fold generations in all (F_1, F_2 and F_3). Belasy's (1991) structural scheme involved an additional folding event between Hegazi's F_2 and F_3. A correlation of Feiran–Solaf with other gneissic complexes of the Eastern Desert on the basis of structure was attempted by Abdel-Meguid (1992). He found that the Feiran–Solaf gneisses had an originally
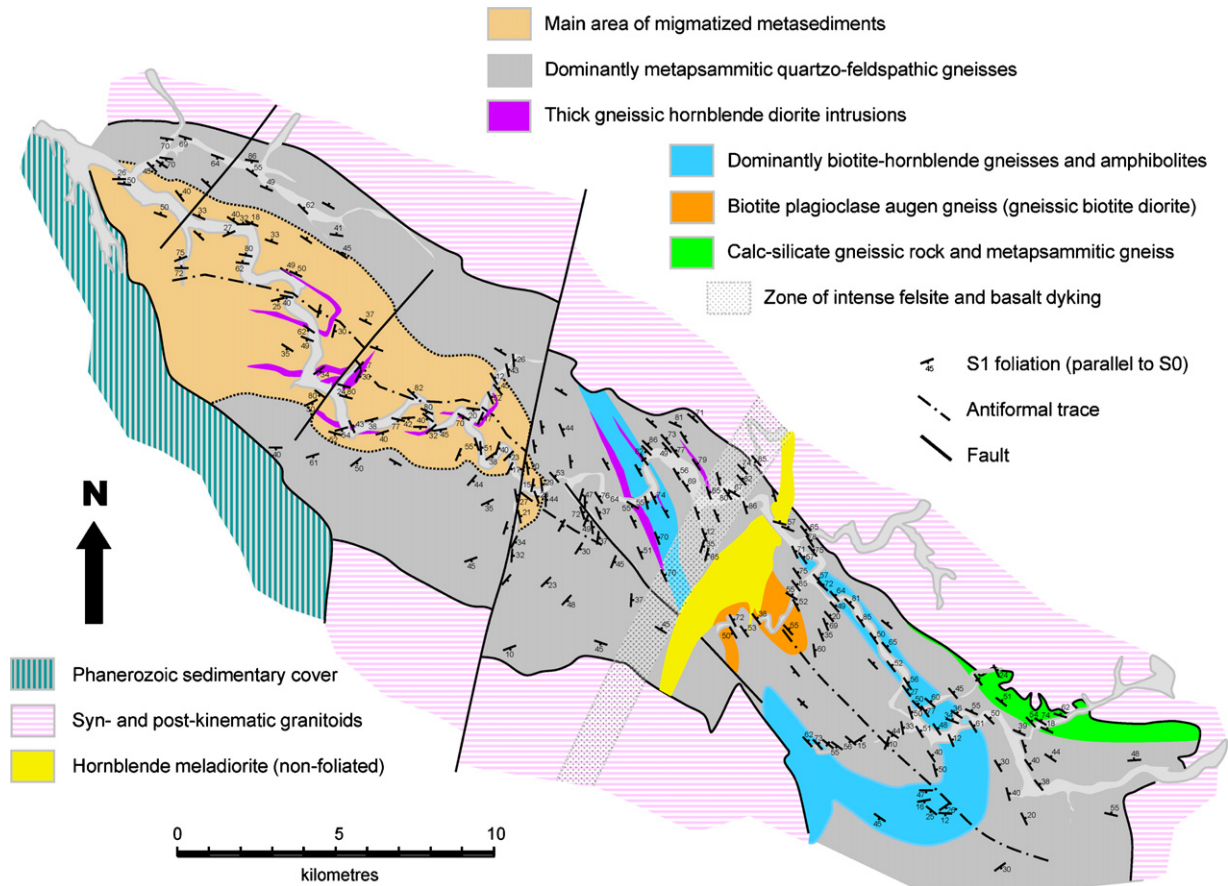
Fig. 2. Geological map of the main lithologies of the Feiran–Solaf metamorphic belt. Representative S_1 foliations orientations at various locations are also shown. Syn- and post-kinematic granitoids are not differentiated in this figure. Some foliation data in the areas distant from the wadis come from Akaad et al. (1967a,b) and Ahmed (1970).

sub-horizontal foliation that experienced later NNW-SSE folding. El-Shafei (1998) came to similar conclusions to Hegazi (1988) though argued that, while M2 was hotter than M1, they were stages of a single metamorphic event during which two major fold generations (F_1 and F_2) developed, the third folding event (F_3) being minor. Khawasik (1995) also reported two significant early and one minor late fold phase in the calc-silicate rocks of Wadi Solaf. Sultan (2003) and Hegazi et al. (2004) returned to the scheme of Belasy (1991), involving four fold deformations with the first three being coaxial. The most detailed structural analysis of the Feiran–Solaf gneisses is by El-Shafei and Kusky (2003). They confirmed El-Shafei's (1998) model in concluding that the Feiran–Solaf macrostructure could be explained essentially in terms of F_1 and F_2 macroscopic fold interference patterns.

3. Geology of the Feiran–Solaf area

The Feiran–Solaf gneisses are bordered to the NE by syn-kinematic granitoids and to the SW by post-kinematic granites and Phanerozoic sedimentary cover as shown in Fig. 2. The main lithological units are metapsammitic quartzofeldspathic paragneiss and biotite-hornblende paragneiss with generally minor but locally abundant intercalations of amphibolite, calc-silicate gneiss and biotite schist. Migmatized metapsammite is widespread in the NW reaches of Wadi Feiran. Apart from the numerous granitic and pegmatitic dykes and sills that pervade these gneisses there are also some thick (10's to 100 m-thick) sills of feebly to strongly gneissic

porphyritic biotite diorite (e.g. Wadi Rimm) and hornblende diorite (mainly in Wadi Feiran).

The lithological map units and the orientations of gneissosity trace out two large antiformal folds—the WNW trending Feiran Antiform, and the NW trending Solaf Antiform. Both folds have broad hinge zones. The Feiran Antiform has a steep SSW dipping axial plane while the Solaf Antiform has an approximately upright axial plane. Both antiforms plunge gently to moderately (20–30°) to the E or SE. Contrary to previous reports (Ahmed, 1970, 1981; El-Shafei and Kusky, 2003) there is no evidence for a synformal structure between these antiforms.

Following the intrusion of tonalite-granodiorite batholiths and Younger Granites, faults formed including NE to NNE trending steep dextral faults (e.g. along Wadi Agala) and a NW-trending steep sinistral fault along Wadi Aleiyat. Cross-cutting the faults are late dykes especially a NE-trending swarm of thin basaltic and red felsite dykes centred on Wadi El Akhdar, and a massive porphyritic hornblende meladiorite dyke to its east.

4. Structure

In this section the individual mesoscopic structural elements of the Feiran–Solaf rocks are described first, with reference to relevant petrographic and microstructural data. This contribution focuses on the structures formed during the development of the gneissosity, in order to better understand its tectonic setting. For this reason we only briefly describe the structural elements that post-date the gneissosity.

4.1. Mesoscopic structures

4.1.1. S_0 lithological layering

Lithological bands with thicknesses ranging from <1 cm to several metres are an important feature, particularly of the Solaf gneisses. They are defined mainly by large differences in percentage and type of mafic minerals. Good examples are thin continuous layers of amphibolite or calc-silicate rock within metapsammites. This banding has long been recognized as sedimentary in origin, and this is consistent with the petrological evidence that the gneisses represent high T metamorphosed pelitic, psammitic and calcareous sediments, which would normally show well-developed stratification. Evidence supporting the primary origin of the lithological layering includes (1) the bands are highly continuous, parallel-sided and have a range of contacts from sharp to gradational; (2) the main differences between the bands are compositional. Phases like sillimanite that are sensitive to rock composition are confined to bands; (3) the banding does not have the characteristics of transposed layering and (4) the banding is not demonstrably younger than any other structure.

4.1.2. S_1 gneissosity, schistosity and migmatitic banding

The combination of strain, metamorphic differentiation and recrystallization has produced a tectonic foliation (schistosity, gneissosity and migmatitic banding), termed S_1, and a mineral lineation L_1 on the S_1 surface (Figs. 3 and 4a, c). In all exposures away from intrafolial folds the S_1 foliation exactly parallels the S_0 lithological layering.

The characteristics of S_1 and L_1 vary greatly depending mainly on rock mineralogy and grain size. Metapsammites with low content of mafic minerals show uniformly distributed mafic grains with preferred orientations (Fig. 3a) and large quartz grains elongate parallel to S_1 (Fig. 3e). Rocks richer in mafic minerals develop penetrative S_1 schistosity (Fig. 3d) or gneissic banding (Figs. 3c and f and 4a). Migmatization is widely developed in the Feiran metapsammites. Migmatized metapsammites have significantly more K feldspar than non-migmatitic ones. K feldspar is concentrated mainly in granitic leucosomes. Melanosomes are enriched in biotite and hornblende.

The S_1-concordant granitoid intrusions show a broader morphological range of gneissosity than the metasediments, because there are several sources of banding in these rocks apart from metamorphic differentiation. These include the stretching out of quartz, feldspar or mafic grains and clots, stretching of xenoliths (Fig. 4d), development of augen from phenocrysts, magmatic flow banding (Fig. 4e) and flow differentiation (pegmatitic streaking in granites). Orientation data for S_1 and S_0 combined is shown in Fig. 5, where it is clear that the poles to these surfaces define great circle girdles on the stereograms for total data, Feiran data and Solaf data. The
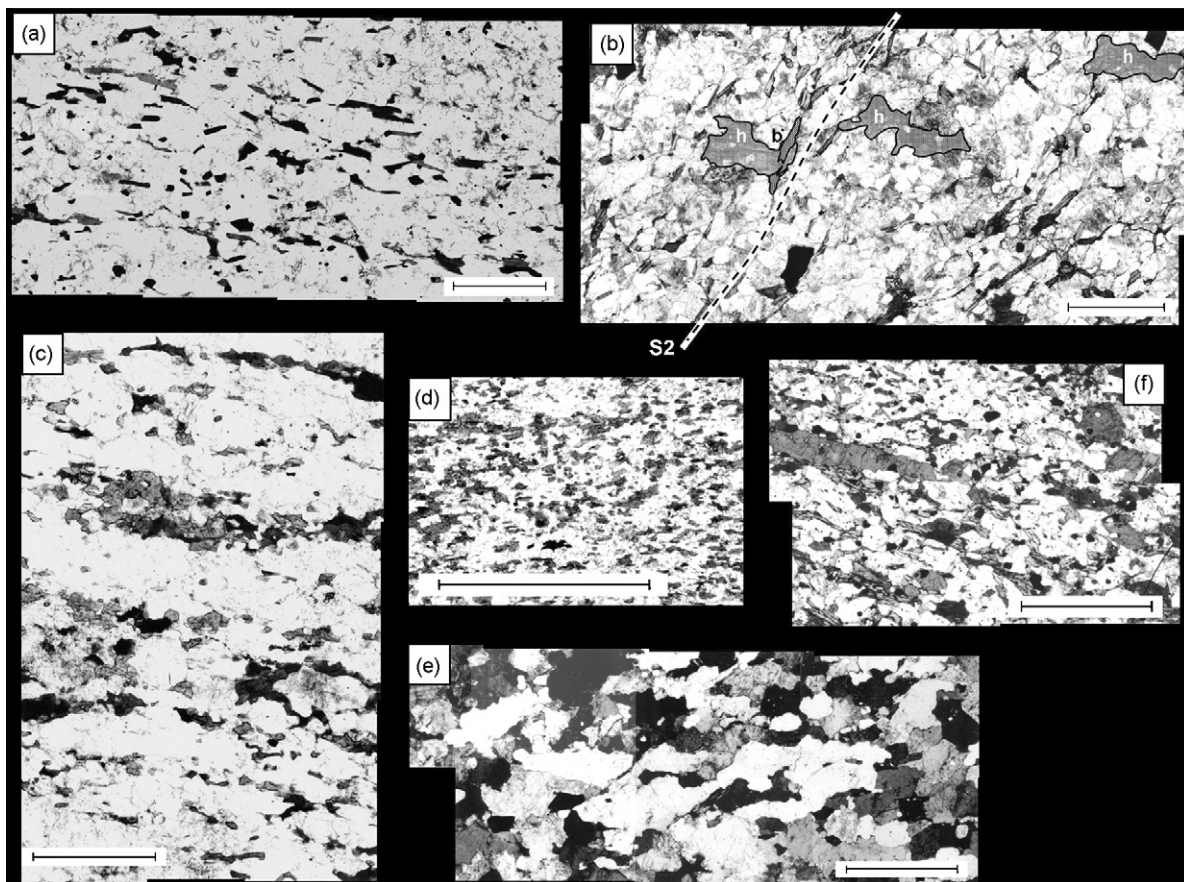
Fig. 3. Photomicrographs of rocks from the Feiran–Solaf area. All photographs except (e) are viewed in plane polars. All scale bars are 1 mm in length. (a) Metapsammitic biotite gneiss from Wadi Um Takha showing S_1 foliation defined by separate parallel oriented biotite flakes. (b) Hornblende biotite gneiss from the hinge zone of an F_2 fold in Wadi Feiran. The long axes of elongate hornblende grains (h) lie along the S_1 foliation (compare with figure f) which is cut at a large angle in the hinge zone by S_2 biotite foliation (parallel to the dashed line). Biotite grains cutting through a hornblende grain are outlined and labelled b. (c) Hornblende gneiss from Wadi Solaf showing gneissic folia defined by hornblende aggregates. (d) Biotite schist from Wadi Um Takha. (e) Quartz-rich metapsammitic gneiss from Wadi Al Akhdar (crossed polars) showing subparallel elongate quartz grains helping to define the S_1 foliation. (f) Hornblende biotite gneiss from Wadi Solaf showing elongate hornblende and biotite defining the S_1 foliation. The rock also resembles a schist in having abundant biotite and fissility along S_1.
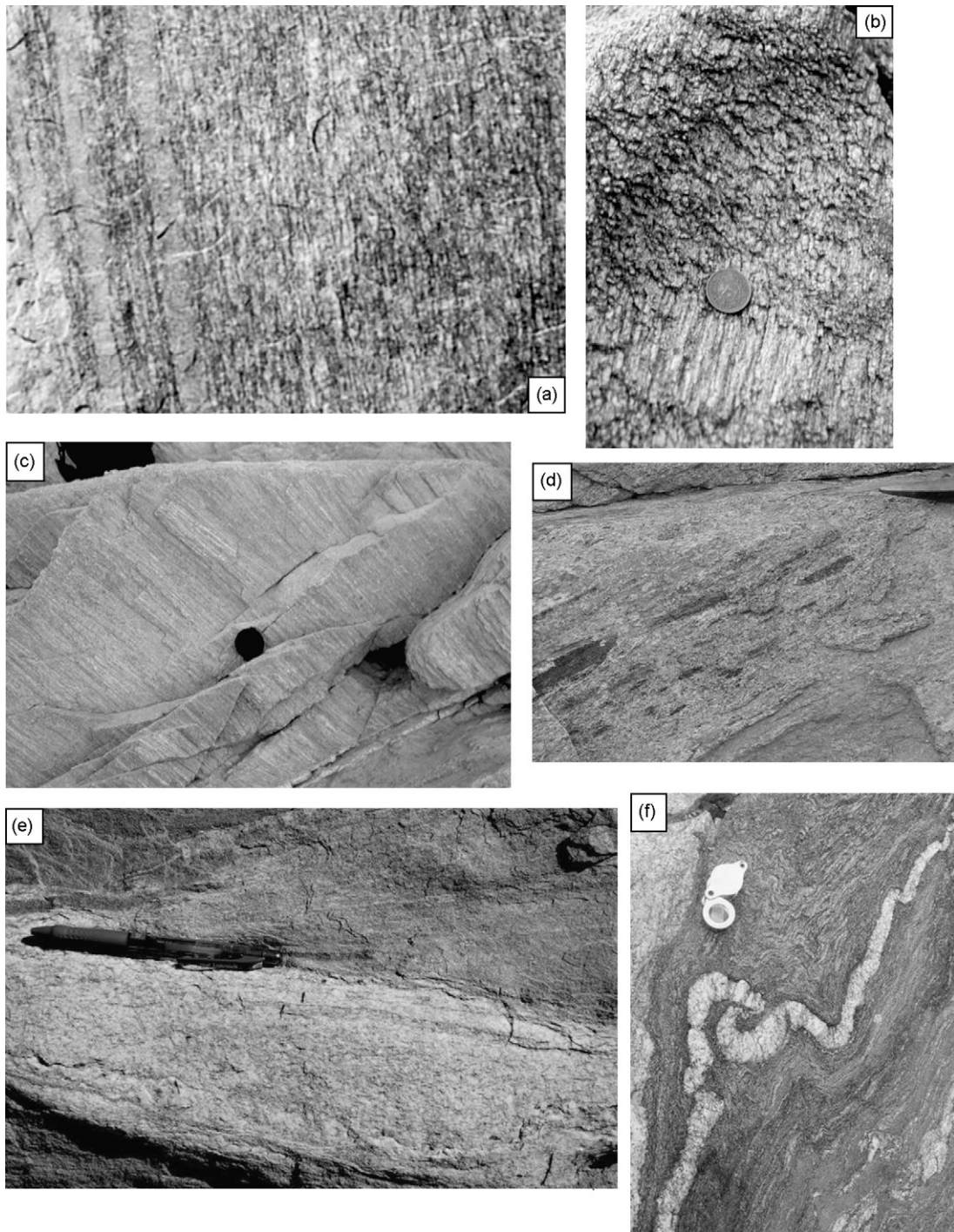
Fig. 4. Field photographs from the Feiran–Solaf area. (a) Well-developed S_1 gneissosity in biotite-hornblende gneiss in Wadi Solaf, (b) L_1 lineation in metapsammite in Wadi Solaf showing a strong linear fabric defined by rod-like domains of quartz, (c) strong L_1 lineation on S_1 foliation in Wadi Solaf. The L_1 lineation provides a surface relief, (d) amphibolite xenoliths in an S1-concordant gneissic diorite in Wadi Feiran, (e) S_1-discordant granitoid dykes in Wadi Solaf showing flow-related gneissosity parallel to its margins and (f) example of F_1/F_2 mesoscopic fold interference pattern in a granitoid dykelet in Wadi Feiran migmatites.

stereograms show the effects of macroscopic folding of S_1 and S_0 (Fig. 2).

4.1.3. L_1 lineations

L_1 is a mineral lineation that is evidently a stretching lineation. Evidence for stretching along L_1 includes the elongation of depletion haloes around porphyroblasts in metasediments and stretching of mafic clots in metadiorites. L_1 is defined by (a)

preferred orientation of the long axes of biotite and hornblende grains; (b) parallelism of lath- or rod-shaped quartz-rich domains in metapsammites (Fig. 4b and c) and (c) parallel highly continuous cm-wide stripes or bands of dark (biotite and hornblende) and light (quartz and feldspar) mineral aggregates. (b) and (c) are essentially types of rodding linear structure, with (c) resembling the ribbon lineations described by Hatcher (1995). Park (1997) noted that rods may be stretching lineations. The characteristics (a)–(c)
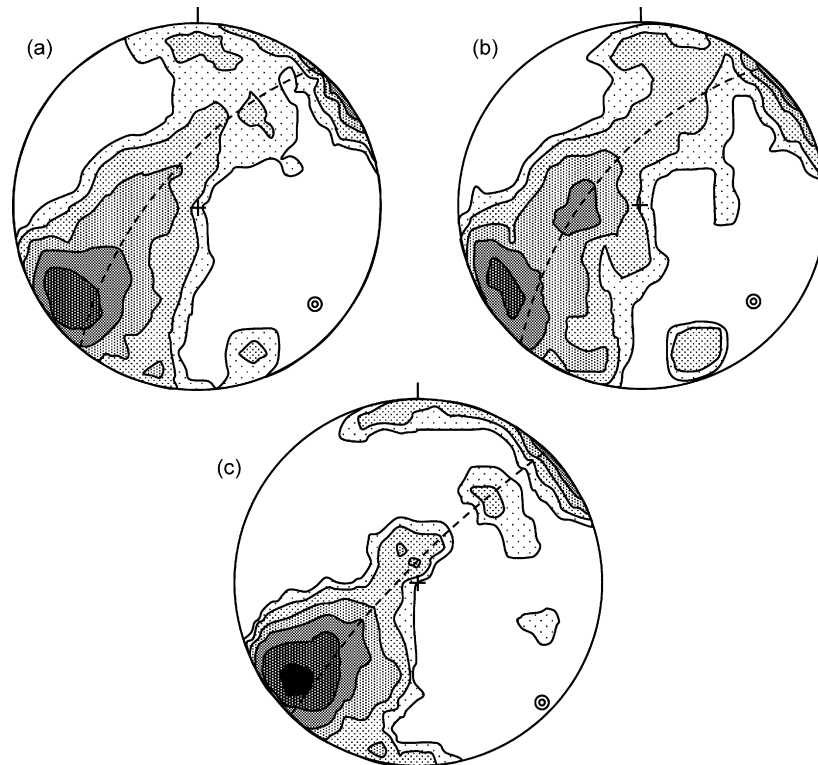
Fig. 5. Stereographic plot of poles to S_1 foliations (lower hemisphere, Schmidt net). (a) 334 poles to S_1 for the entire Feiran–Solaf study area. Point density contours are at 1%, 2%, 4%, 8% and 16%. β-axis plunges 18° towards S50E. (b), 198 poles to S_1 for the Wadi Feiran area. Point density contours are at 1%, 2%, 4%, 8% and 16%. β-axis plunges 21° towards S49E. (c) 132 poles to S_1 for the Wadi Solaf area. Point density contours are at 1%, 2%, 4%, 8%, 16% and 32%. β-axis plunges 7° towards S46E. All stereograms show great circle girdle distributions. Girdle is shown as dotted line, with girdle (β) axis indicated by small annulus symbol.

of L_1 correlate well with the features of S_1, so that for example, (b) is characteristic of the quartz-rich metapsammitic gneisses and (c) is typical of the hornblende-biotite gneisses.

L_1 typically uniformly pitches 20–50° to the NW or SE on S_1 in any continuous exposure. In some single exposures the L_1 pitch angle ranges from 15° to 60° (in the same pitch direction) over a distance of 10 m along strike of S_1 and only 1 m thickness of gneissic rock. This local variation is not due to folding of S_1, so it appears that the L_1 lineation is locally curvilinear within the planar S_1 foliation. On the regional scale, the total L_1 lineation data shows two concentrations on the stereogram: one characterized by gentle NW plunges and the other with gentle SE plunges (Fig. 6a). The SE plunging L_1 data is mainly from Wadi Feiran (Fig. 6b), while the NW plunging L_1 data is mainly from Wadi Solaf (Fig. 6c). See Section 5.1 for discussion of these patterns.

4.1.4. F_1 folds

Previous reports of the F_1 folds of this area have described F_1 as small, tight to isoclinal, rootless and intrafolial folds with sharp hinges parallel to the L_1 stretching lineation, and plunging gently to the SE (Hegazi, 1988; El-Shafei, 1998; Sultan, 2003; El-Shafei and Kusky, 2003; Hegazi et al., 2004). These same studies also identified an overprinting set of coaxial folds (F_2) with approximately the same style as F_1 (tight to isoclinal "similar" folds with angular hinges parallel to L_1), and relied on fold orientation and fold interference patterns to distinguish F_1 from F_2. F_1 and F_2 were also grouped within one deformation event (termed D1) spanning a single regional metamorphic event (M1—amphibolite facies). Distinguishing between F_1 and F_2 folds on the basis of orientation is not a good practice, and is pointless, since F_1 and F_2 are coaxial. There are not enough examples of interfering F_1 and F_2 mesoscopic folds to routinely use this to identify F_1 and F_2 (Fig. 4f). It appears

that most of the folds illustrated by El-Shafei and Kusky (2003) as F_1 folds are actually F_2 folds (see Table 1), on the basis that their folds are not intrafolial, they fold S_1, and show no features indicating that they are syn-gneissosity.

We believe it is better to define F_1 as folds that were evidently formed by the same deformation event as the S_1 foliations, as is true for most deformed terrains. We have not seen any examples that show two fold generations, one folding the other, with both generations being clearly syn-S_1.

Using the above definition for F_1 folds, there appears to be more than one style of F_1 folds (Fig. 7a–c). All are intrafolial with respect to S_1, and they are typically tight to isoclinal, usually have thickened hinge zones, attenuated limbs, and sometimes ptygmatic style. F_1 folds have hinges parallel to the L_1 stretching lineation (Fig. 6a and d) and axial planes at a small angle to the S_1 foliation. We will return to the question of how to recognize S_1-related strain as a cause of F_1 folding in Section 4.4. Other aspects of F_1 folds, e.g. fold asymmetry are also deferred until that section.

4.1.5. Boudins

A widespread feature of the Feiran–Solaf area are boudins and pinch-and-swell structures that have developed in the plane of the S_1 foliation (Fig. 8). Amphibolite boudins (Fig. 8g) locally show complex brittle effects accompanied by granite or pegmatite injections. Foliation boudins, such as those described by Platt and Vissers (1980) are also present. Boudin outlines are seen in all sections normal to S_1 including those parallel and at right angles to L_1 (Fig. 8a and b). This indicates that these structures have geometry consistent with chocolate tablet boudinage, as noted by El-Shafei (1998). Lenticular boudins formed by attenuation of pinch-and-swell are the commonest boudin shapes in cross-section. Such cross-sectional shapes normally indicate lensoidal boudin geom-
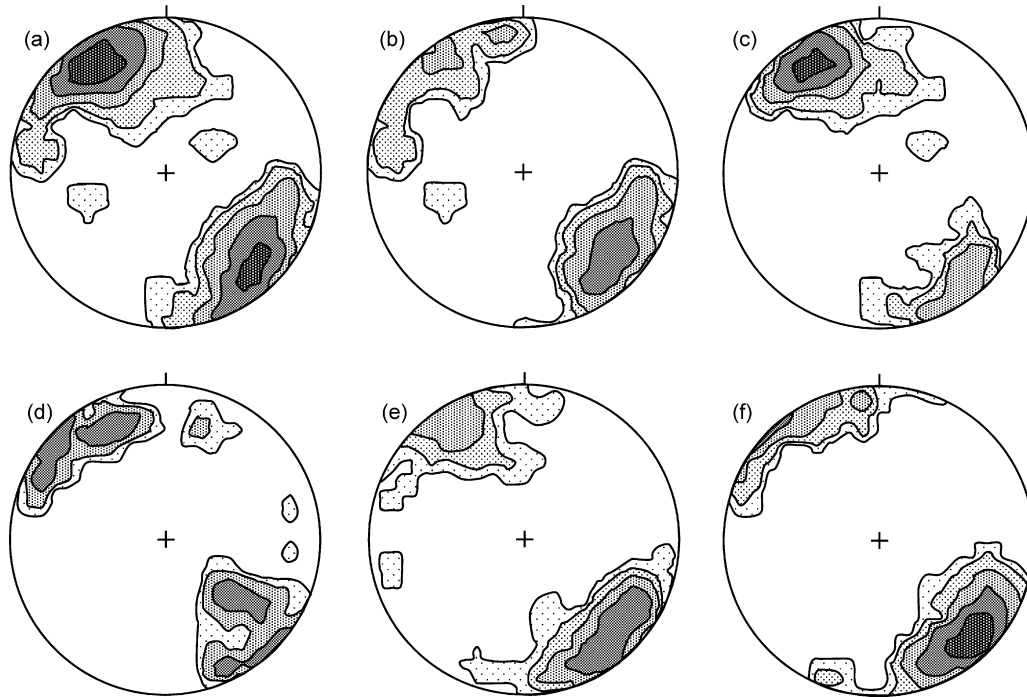
Fig. 6. Stereographic plot of linear data (lower hemisphere, Schmidt net). (a) 144 L_1 lineations for the entire Feiran–Solaf area. Point density contours are at 1%, 2%, 4%, 8% and 16%. (b) 67 L_1 lineations for the Wadi Feiran area. Point density contours are at 2%, 4%, 8% and 16%. (c) 77 L_1 lineations for the Wadi Solaf area. Point density contours are at 2%, 4%, 8%, 16% and 32%. (d) 35 F_1 fold hinges for the entire Feiran–Solaf area. Point density contours are at 3%, 6% and 12%. (e) 88 F_2 fold hinges for the entire Feiran–Solaf area. Point density contours are at 2%, 4%, 8% and 16%. (f) 58 F_3 fold hinges for the entire Feiran–Solaf area. Point density contours are at 2%, 4%, 8%, 16% and 32%.

etry in three-dimensions (Fig. 8d). According to Ghosh (1988) lensoidal boudins with round shape in plan view are indicative of flattening strain in the plane of the boudins, produced by simultaneous extension parallel and at right angles to the stretching lineation. This is probably the origin of the Feiran–Solaf boudins because (1) the uniform array of hummocky swells is not consistent with segmentation of earlier cylindrical pinch-and-swell and (2) there are no obvious differences in the geometry (aspect ratio, tapering angle, etc.) and structural relations of the pinch-

and-swell structures in the sections parallel and perpendicular to L_1.

The commonest boudins in the study area are symmetrical and result from approximately layer-parallel coaxial extension. Rhomb-shaped asymmetric boudins are associated with extensional shear dissection of the layers (Fig. 8e). These shear boudins also experienced varying degrees of back-rotation so that S_1 within the boudin may lie at a large angle to S_1 in the layers above and below (Fig. 8h). The asymmetric boudins illustrated by El-Shafei (1998, Fig. 45a)

Table 1
Comparison of the structural terminology of El-Shafei and Kusky (2003) and of this study

Description of the element	El-Shafei and Kusky (2003)		This study		Comments
High grade foliation including gneissosity, migmatitic foliation, penetrative schistosity	S_1		S_1	D1 event	Parallel to S_0 (lithological banding) except in the immediate vicinity of F_1 folds
Small very tight to isoclinal, usually rootless, intrafolial folds. Asymmetry variations vary irregularly even in a single outcrop. Hinges parallel to L_1 stretching lineation	F_1		F_1		In our study these folds must be convincingly syn-S_1. Fold asymmetries do not support the existence of macroscopic folds or of regional shearing at this stage
Tight to almost isoclinal folds harmonically folding the S_1 foliation. Axial planes at a moderate to low angle to S_1 foliations. Axial plane cleavage S_2 is a close-spaced foliation but not gneissic or migmatitic. Fold asymmetries support the existence of small macroscopic folds. Hinges are *generally* parallel to L_1	Most of their figures of fold interference present these as F_1	D1 event	F_2	D2 event	These folds have variable shape and interlimb angle. They commonly have small ductile shears on one limb and appear to be related to regional NE-SW shortening and SW-ward thrusting. L_1 is locally refolded by these folds and the axial plane cleavage S_2 cross-cuts L_1. S_2 is post-gneissosity
Commonly upright but locally inclined, open to close folds. They show a low-grade spaced crenulation parallel to the axial plane	Most of their figures of fold interference present these as F_2		F_3	D3 event	Away from earlier folds it is clear that these folds are generally symmetric. Their intensity and style variations correlate with their position on the Feiran and Solaf antiforms (tighter and upright in the hinge zones of the Feiran and Solaf antiforms and more open and inclined on their limbs)
Open steeply plunging folds with consistent NE-SW to E-W axial planes. Some take on a kink-like appearance. Feeble crenulation along the hinge may be present	F_3	D2 event	F_4	D4 event	Consistent with NW-SE minor shortening
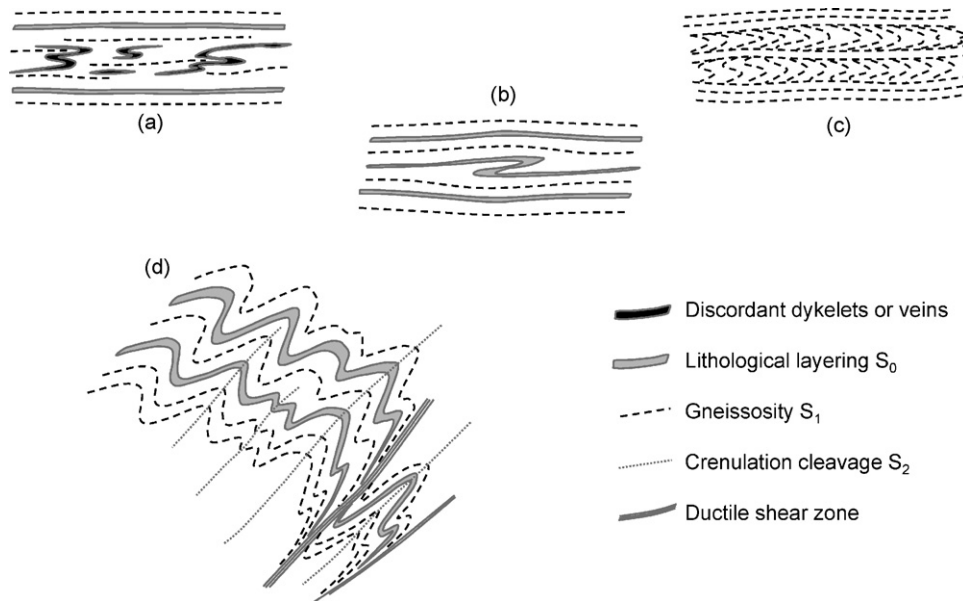
Fig. 7. Idealized sketches of types of F_1 folds (a–c) and F_2 folds (d), showing essential characteristics. (a) Rootless intrafolial F_1 folds developed in originally discordant dykelets and veins. (b) Intrafolial F_1 folds in continuous lithological layers (or concordant intrusions). (c) "Intrafolial" F_1 folds in S_1 foliation terminated above and below by S_1 foliations. (d) F_2 folds showing variable interlimb angles, harmonic to "similar" style, shearing along limbs, and crenulation axial plane cleavages.

are not indicators of a shear strain regime. They formed in veins that were discordant to S_1 but within the elongation sector of the strain ellipse associated with S_1. Their asymmetric shape and *en échelon* orientation are due to oblique extension combined with rotation of the boudin array and the individual boudins towards the *XY* plane occurring at different rates (Price and Cosgrove, 1990, their Fig. 16.40) (Fig. 8f).

4.1.6. Extensional ductile shear zones

The ideas of early (D1) regional scale shearing/thrusting in the tectonics of the Feiran–Solaf area proposed by previous workers will be discussed later. Here we describe the characteristics of mesoscopic ductile shear zones that appear to have formed during S_1 development (Fig. 9). The normal-sense ductile shears associated with asymmetric boudin formation, mentioned in the previous section, are examples of shears active during S_1 development. The shears are also found to extend well beyond the boudin-affected layers (Fig. 8c and h). These D1 ductile shears are commonly curved (concave upwards) leading to roll-over rotation of S_1 foliations near the shear plane (Fig. 8h). The shears curve into parallelism with the S_1 foliation both upwards and downwards so that the discordant part of the shear passes through only about a metre or so of S_1 foliated rock.

The normal-sense ductile shears commonly lie at 30° to the layering and S_1 (Fig. 9d). The S_1 foliation in the hanging wall of the shear lies at a small angle to the shear plane while the shear is discordant to the S_1 foliation below (Fig. 9a). There are conjugate senses of shear in the same locality. Most of the shears were found in exposures along wadis lying at a large angle to the trend of L_1 (e.g. Wadis Agala and Aleiyat). This is probably because the line of intersection of the shear plane with S_1 is most often roughly parallel to the L_1 lineation (Fig. 9b). The drag and rotation effects on S_1 and compositional layering in the hanging walls, however, indicate that the shear couple lies in the S_1 plane but is roughly at right angles to L_1. These unusual features are considered later in the context of the evolution of the boudins and F_1 folds. Poles to the D1 extensional ductile shears are plotted stereo-

ographically in Fig. 9c. See Section 5.1 for consideration of this diagram.

### 4.1.7. F_2 folds and S_2 foliations

F_2 folds are "similar" style folds that fold the S_1 foliation. They tend to harmonically fold many layers and are not intrafolial like F_1 folds (Fig. 10a). F_2 folds in thick bodies of migmatitic or gneissic rocks show highly variable interlimb angles and profile shapes, even within a single train of folds (Figs. 7d and 10a). At larger interlimb angles the F_2 folds tend to be polyclinal, but their axial planes become more closely parallel as their interlimb angles decreases. Their hinges are mainly though not exclusively parallel to L_1 (Fig. 6a and e), but on close inspection it can be seen that the L_1 lineation and S_1 foliation are interrupted and deformed by the S_2 spaced cleavages that are locally developed along tight F_2 fold axial planes (Fig. 3b). A common feature of these folds is the development of ductile shears along one limb (Figs. 7d and 10b). These shears are commonly intruded by foliated granites. F_2 folds have been described as being related to thrusting to the SW by El-Shafei and Kusky (2003) and Hegazi et al. (2004), and a SW-vergent major thrust of F_2-age lies along the NE border of the Feiran–Solaf gneisses.

4.1.8. F_3 and F_4 folds and crenulations

Two generations of gentle to close folds post-date F_2. F_3 folds have rather concentric style (Fig. 10e) and their hinges again are roughly parallel to L_1 (Fig. 6a and f), as found by Sultan (2003). They fold S_0 and S_1, and there are some good examples of F_2/F_3 interference patterns where F_3 folds the F_2 axial planes (Fig. 10c–e). El-Shafei and Kusky (2003) did not distinguish these folds from F_2 folds, despite the F_3 folds being post-, not syn-high grade M1 metamorphic structures (Table 1). As a result (and in combination with their representation of many F_2 folds as F_1) the fold interference patterns they designated as F_1/F_2 are really F_2/F_3. The tighter F_3 folds have a weak crenulation along their hinges. F_4 folds appear always to be open fold structures (Fig. 10g). They have NE-SW to E-W trends and steep plunges and were referred to as F_3 by El-Shafei and Kusky (2003) (Table 1). They are not common structures.
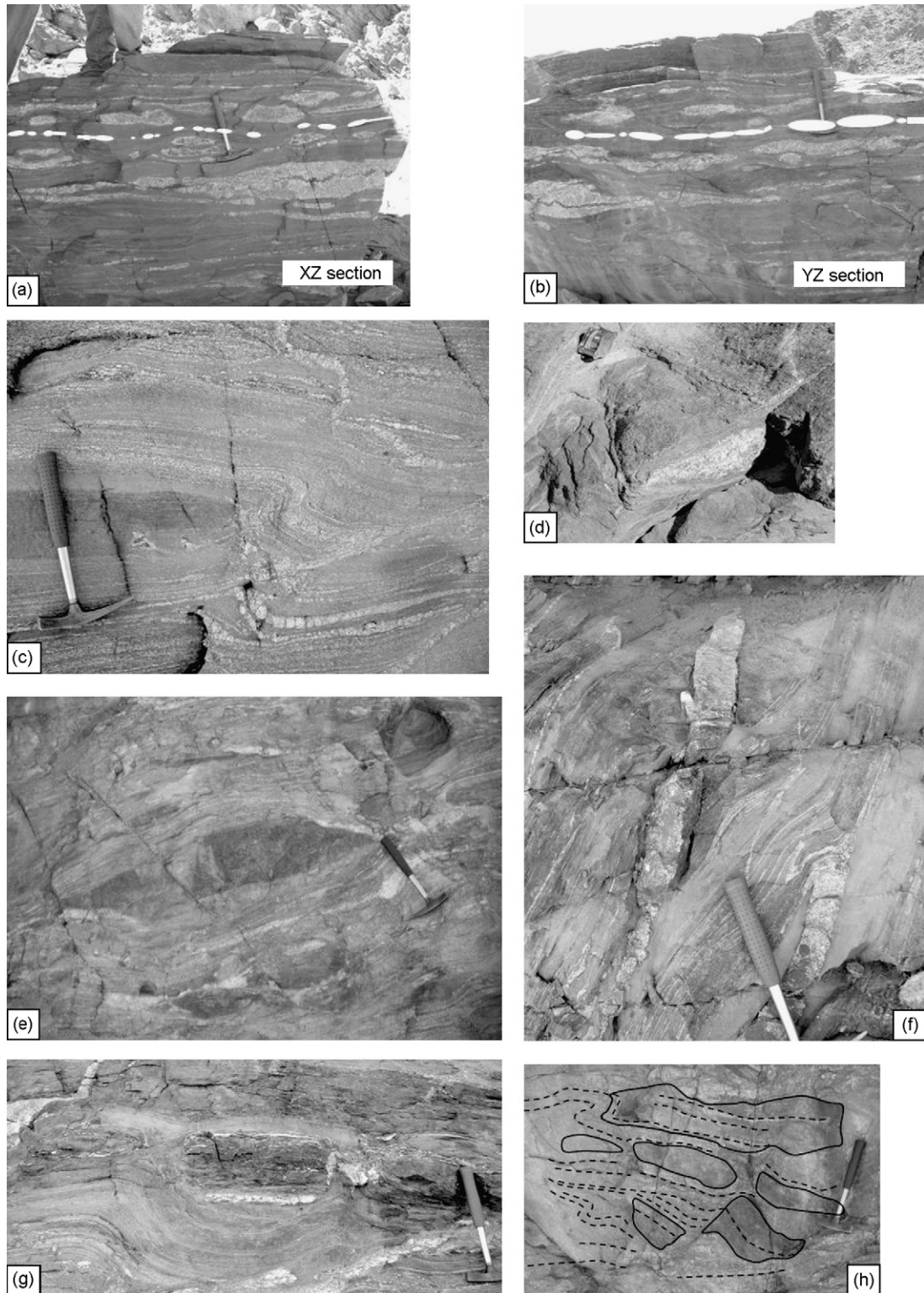
Fig. 8. (a) A fallen block of granitoid intruded hornblende-biotite gneiss in Wadi Solaf. The exposed joint face is approximately parallel to L_1 and right angles to S_1 making it close to the *XZ* plane of strain. A boudinaged layer is highlighted in white. Extension in the *X* strain direction based on this layer of boudins is estimated to be 214%. The method assumes no dilatation on this plane, and that the original layer was at least as thick as the thickest boudin. The area of boudins is calculated and divided by the original layer thickness to obtain the original layer length parallel to S_1, which is then compared to present length of the boudin array. (b) Same block as (a) but looking on another joint face normal to L_1, making it close to the *YZ* plane of strain. Same method as for (a), based on the same boudinaged layer as for (a), gives an extension in the *Y* direction of 152%. (c) Boudin of amphibolite lying to the left of an extensional ductile shear that passes downwards into parallelism with S_1. The F_1 fold to the upper right of the boudin is probably a product of back-rotation on the extensional shear combined with continued shortening normal to S_1 (Wadi Agala). (d) Lensoid shape of boudins in 3D (Wadi Solaf). (e) Rhomboid boudin of amphibolite produced by extensional shear failure. Note the pegmatitic material at the boudin terminations (Wadi Agala). (f) Asymmetric boudin (left of centre) formed by oblique extension of a granitoid dyke discordant to S_1 (Wadi Feiran). (g) Symmetric boudins of amphibolite in migmatitic metapsammite (Wadi Feiran). (h) Boudin, F_1 fold and extensional shear relations in metapsammitic gneiss (Wadi Agala). Note the back-rotation of boudins and foliations in the lower third of the photograph. F_1 folds here are produced by shortening of the back-rotated foliations.
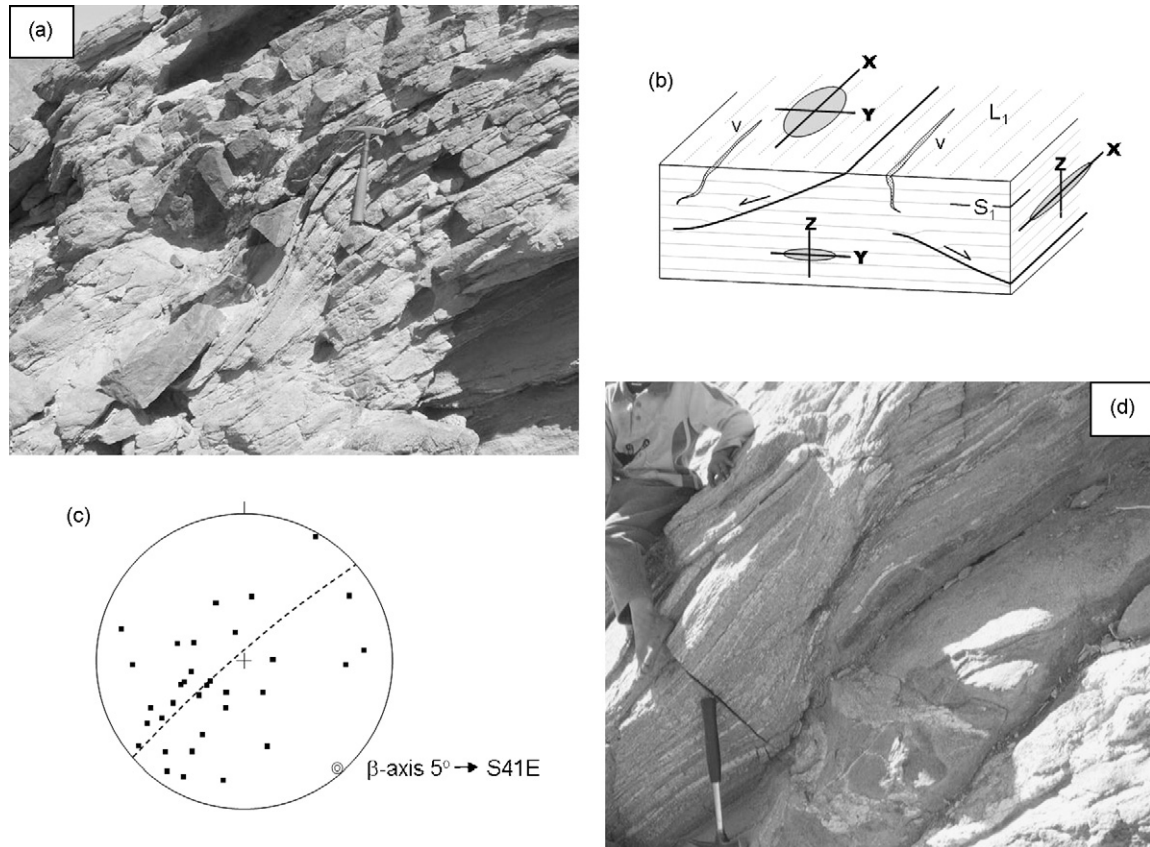
Fig. 9. D1 extensional ductile shears. (a) Looking east at a NE dipping extensional ductile shear lying at 35° to S_1 (Wadi Feiran). (b) Block diagram showing the geometrical relations of the extensional ductile shears and syn-S_1 dykes and veins (v) to S_1 and to the bulk principal strain axes X, Y and Z. (c) Stereographic plot of 33 poles to extensional ductile shears (lower hemisphere, Schmidt net). Girdle distribution is shown with girdle (β) axis indicated. (d) Looking south at an E-dipping extensional ductile shear lying at 35° to S_1 (Wadi Feiran).

4.2. Strain in the gneisses

The S_1 foliation and L_1 lineation rock fabric elements appear to be parallel to the *XY* (flattening) plane and maximum extension direction *X* of the bulk finite strain ellipsoid for the Feiran–Solaf gneisses (Fig. 9b), as has been found for gneissosity in other regions (Lacassin and Van Den Driessche, 1983; Odling, 1984; Soto, 1991; Mulchrone, 2002). Evidence for flattening parallel to S1 includes the mainly symmetrical form of boudin and pinch-and-swell structures in S_1; axial planes of isoclinal F_1 folds lying parallel to S_1 and S_1 related elliptical depletion haloes about porphyroblasts having long axes parallel to S_1. Features indicating stretching parallel to L_1 include elongation of depletion haloes, long axes of quartz mineral aggregates and stretched xenoliths, and a parallelism of long axes of mineral grains to L_1. As noted in Section 4.1, the S_1 foliation is typically parallel to the lithological layering (S_0). From this it follows that the bulk strain ellipsoid has maximum shortening direction *Z* normal to the lithological layers (Fig. 9b).

Boudins may also be useful for estimating strain in gneissic rocks. The layer of chocolate tablet boudins shown in Fig. 8a and b affords measurement of extension in both the *X* and *Y* directions. These give $X \sim 214\%$ and $Y \sim 152\%$. Assuming no dilatation, *Z* is calculated to be $\sim -79\%$ normal to the S_1 gneissosity. This gives $R_{XZ} = 14.9$, $R_{YZ} = 7.2$, and $R_{XY} = 2.1$. The *k* value for this strain ellipsoid is 0.18, i.e. clearly a triaxial strain lying in the flattening field. This strain estimate is a minimum since it records only the strain accumulated since the intrusion of the veinlet.

Strain ellipses for principal sections *YZ* and *XY* were also estimated, for example, stretched xenoliths in gneissic tonalite from

Wadi Rimm gave $R_{YZ} = 5.7$, whereas depletion haloes from a faintly gneissic microtonalite from the same wadi gave $R_{YZ} = 2.4$. The difference in these values is evidently due to different timing of intrusion of the tonalitic melts with respect to deformation. Elongate mafic mineral aggregates on S_1 foliation from Wadi Um Takher gave $R_{XY} = 3.45$. Although limited, this strain data indicates that the S_1 foliation formed by triaxial flattening strain normal to layers, and that tonalitic, dioritic, granitic melts have intruded at different stages during S_1 formation. Further minimum shortening strain estimates parallel to *Z* are presented in the Section 4.4, using F_1 folds.

4.3. Significance of the D1 extensional shears

The evidence that the extensional shears described in the previous Section 4.2 are D1 in age includes (1) their close association with boudinage in S_1; (2) their parallelism to S_1 in part with no evidence of overprinting of a shear foliation over S_1 and (3) the common injection of pegmatite along them that continues on to inject into boudin necks and separation zones as the boudins formed.

The commonest of these shears in the Feiran gneisses have orientations consistent with those formed by layer-normal shortening illustrated by Platt and Vissers (1980) and Kidan and Cosgrove (1996). The experimental ductile shears characterize moderately anisotropic multilayers while internal pinch-and-swell is preferred at lower anisotropy. No definite internal pinch-and-swell was found in the Feiran–Solaf gneisses.

One of the odd features of the D1 extensional shears is that they intersect the S_1 gneissosity in a line parallel or at a small angle
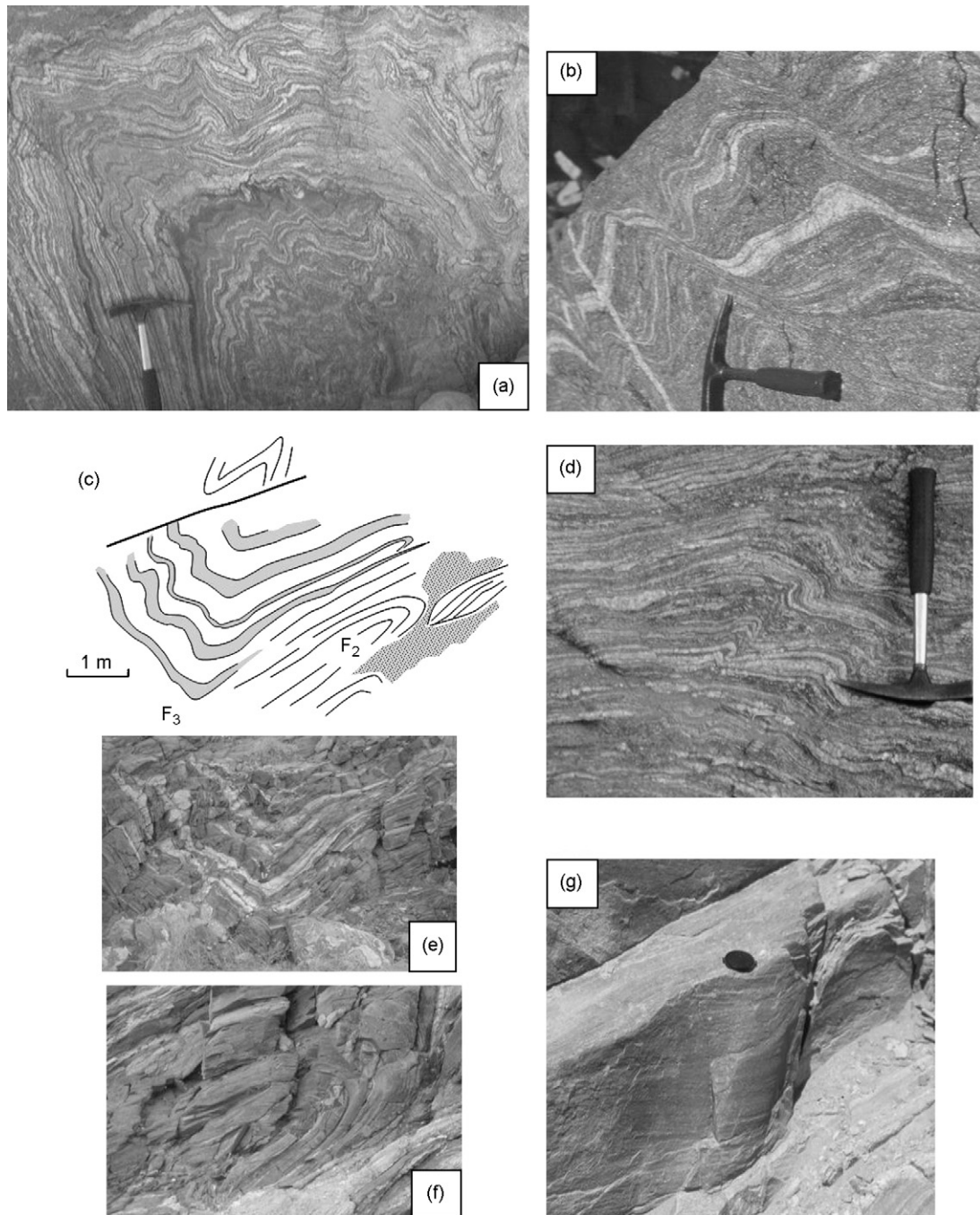
Fig. 10. Field photographs of post-F_1 folds. (a) F_2 folds showing complex variations in fold shape, interlimb angle and axial plane orientation (Wadi Feiran). (b) F_2 folds showing shearing along some limbs (fallen block in Wadi Feiran). (c) Sketch of F_3 folds overprinting F_2 folds (Wadi Feiran). (d) Asymmetric F_2 folds (Wadi Feiran). (e) The F_3 fold sketched in (c). (f) The approximately isoclinal F_2 fold sketched in (c). (g) Steeply plunging F_4 fold folding S_1 and L_1 lineation (Wadi Feiran, near Wadi El-Sheikh).

to L_1. This indicates that the displacement vector for these shears lies at right angles to L_1, parallel to the Y intermediate strain axis (Fig. 9b). As noted above, the Y strain axis was also a direction of extension, but a question that instantly arises is why should the extension direction controlling displacement for these shears be the Y direction rather than the X direction? This is explained below in relation to plastic anisotropy in the XY plane.

4.3.1. Control on the orientation of the ductile shears

The grain fabric of a material has a strong influence on the ductility of that material. The phenomenon of plastic anisotropy (material ductility varying with direction) is well known for metals

with parallel elongate grains, or material composites with embedded parallel fibres. These show a substantially greater ductility parallel to the linear fabric than transverse to it (Canova et al., 1985; Hosford, 1998; Skrotzki et al., 2001). Combination of planar and linear fabric in rolled sheet metals produces a strong in-plane plastic anisotropy (Man, 2002). Comparable plastic anisotropy is found in natural tectonites (Takeshita, 1989; Gottschalk et al., 1990; Wenk and Van Houtte, 2004). Platt and Vissers (1980) noted that foliation in rocks reduces the ductility in tension parallel to it and Ghosh (1988) remarked that there is higher ductility along a stretching lineation than transverse to it in the foliation.

The L_1 stretching lineation in S_1 is exceptionally well-developed throughout the Feiran gneisses, to the point of resembling a bundle of parallel flattened straws of quartz in some metapsammites (Fig. 4b). We believe this strong fabric produced a higher ductility parallel to X than perpendicular to it (in the direction Y). Ductile extensional shear zones are spaced structures initiated at strain softened locations (Poirier, 1980) and are therefore more likely to characterize extensional strain in directions of lower ductility (direction Y) in the rocks, while homogeneous extension is occurring in directions of higher ductility (direction X).

The ductile shear zones with Y direction of displacement are extensional zones of non-coaxial strain enclosed within wall rocks undergoing coaxial deformation. This has involved syn-shearing stretching along the X direction of the wall rocks at right angles to the displacement direction in the shear zones. Such shears are stretching faults (Means, 1989) or laterally expansional shears (Passchier, 1998). For such shear zones the mineral lineations lie parallel to the X direction of the wall rocks rather than along the slip vector of the shear (Passchier, 1998). This is true for the Feiran ductile shears. We will now explain the role of plastic anisotropy in the development of F_1 folds.

4.4. F_1 folding mechanisms

As noted above, the F_1 folds are intrafolial and of three styles (Fig. 7a–c). Ideas for the formation of intrafolial folds can be grouped into two: (1) mechanisms involving shear parallel to the planar layers above and below, leading to shearing along fold limbs, disruption of fold trains and ultimately transposed foliations (Hobbs et al., 1976; Davis, 1984; Hatcher, 1995) and (2) mechanisms emphasizing stretching parallel to layers leading to amplification of some folds, de-amplification of others and disruption of fold limbs at higher strains by boudinage rather than shearing (Ramsay and Huber, 1983). We argue that it is flattening mechanism (2) not shearing mechanism (1) that is responsible for the development of F_1 folds in the Feiran–Solaf area, as explained below.

4.4.1. First style: rootless intrafolial F_1 folds (Fig. 7a)

These F_1 folds are mainly represented by folded dykes and veins which intruded across S_1 foliation during S_1 development (Figs. 7a and 11f, g). Continued flattening normal to S_1 has folded the dykes and veins so that their axial planes are parallel to S_1. The parallelism of the axial planes of this F_1 fold style with S_1 at all
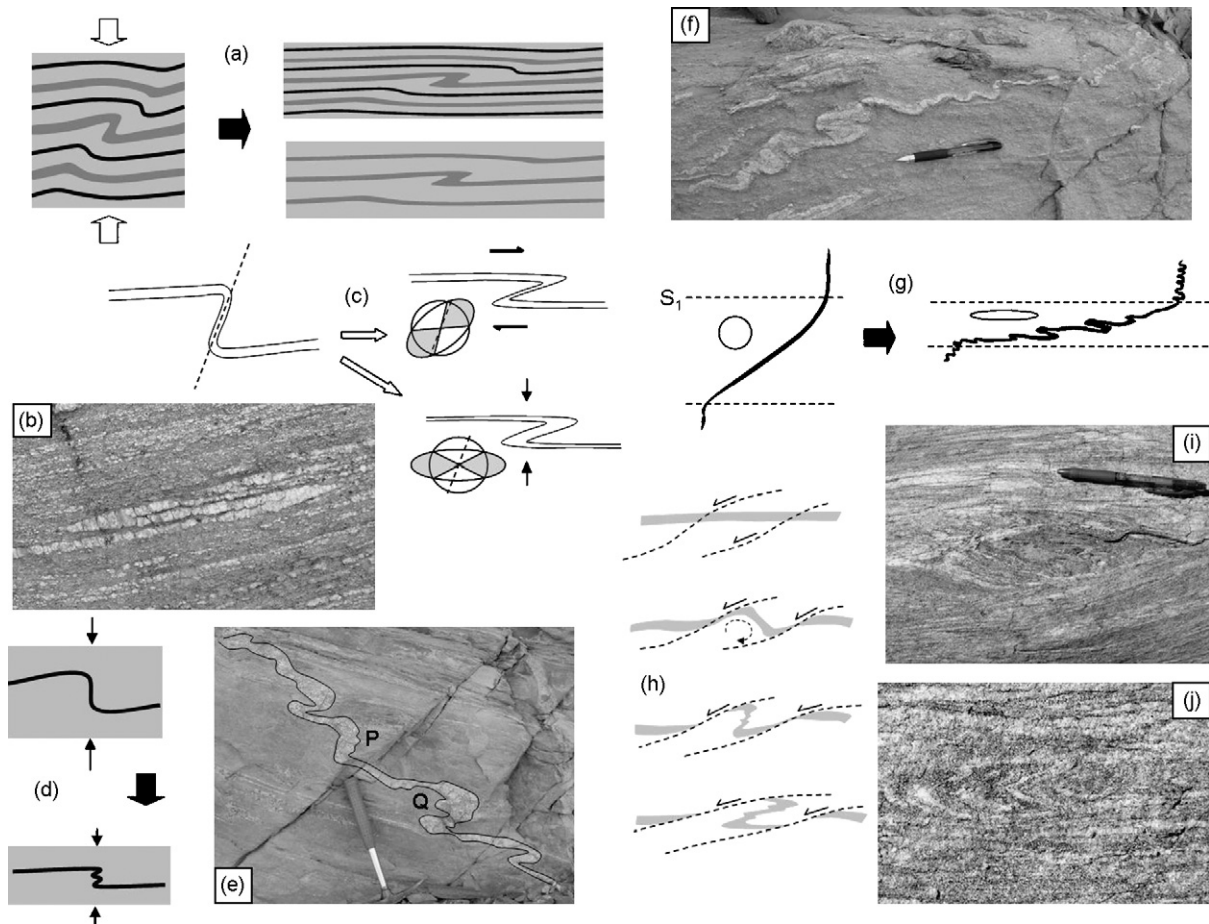
Fig. 11. F_1 folding mechanisms illustrated. (a) Layer-normal shortening of an asymmetric fold with one layer showing a fold with overturned short limb. The overturned fold amplifies and tightens while the folded layers above and below unfold, to produce an intrafolial fold in a continuous layer. (b) Example of (a) developed in a migmatite leucosome (Wadi Feiran). (c) Distinguishing between amplification of intrafolial fold by continued shear parallel to layers (overturned short limb is thinned); and amplification by layer-normal shortening (overturned short limb is thickened) (from Ez, 2000). Dotted line represents original short limb orientation that either lies in the instantaneous extension field (for shearing parallel to layers), or the shortening field (for layer-normal shortening). (d) Buckling of the F_1 asymmetric fold short limb by layer-normal shortening in the case that the short limb is initially vertical rather than overturned. (e) Example of an F_1 folded dyke showing features similar to (d). (f) F_1 asymmetric and ptygmatic folds developed in intruded dykelets (Wadi Feiran). (g) Explanation of the origin of asymmetry for the F_1 folds shown in (f). (h) Development of F_1 folds by back-rotation of layers or foliation on extensional ductile shears as the shears rotate towards the flattening plane (from Harris et al., 2002). (i) Example of back-rotation of S_1 in internal boudin (Wadi Feiran). (j) Example of F_1 folded S_1 foliations themselves truncated by S_1 foliations (Wadi Feiran). These form ultimately by the mechanism shown in (h).

stages of amplification is the evidence for the same-age relations of F_1 and S_1 in this case. The parallelism of these F_1 axes to L_1 will now be explained.

During S_1 development the inferior ductility in the Y finite strain direction controlled the orientation of magma-filled tensional fractures, and veins. Although the initial geometry of these dykes and veins may have been variable their line of intersection with S_1 is parallel to L_1 as shown in Fig. 9b. Ghosh (1993, Fig. 17.22) explained how tensional veining can occur parallel to the strong stretching lineation, while pinch-and-swell forms perpendicular to the lineation, due to in-plane ductility contrast. Continued S_1-normal shortening of the host rock has folded the dykes and veins in a ptygmatic style common to these F_1 folds (Fig. 11f). These folds are rootless and intrafolial not because of disruption of a fold train, but because the original dykes and veins had limited dip length. The asymmetry of these F_1 folds changes according to the angular relations of the original dyke or vein to the S_1 foliation. It is obvious from this model that the F_1 folds formed will have their hinges parallel to L_1.

This type of F_1 fold may be used to estimate strain via the methods outlined in Ramsay (1967) and Lisle (1992) (Fig. 12a–g). The F_1 fold example in Fig. 12 yields a strain ellipse with $R = 2.22$ using Ramsay's method and 2.24 using Lisle's (1992) method. A further shortening of -36% normal to S_1 accounts for the buckling of the folds. Altogether the shortening normal to S_1 since intrusion of the dykes is -57%.

4.4.2. Second style: F_1 folds in continuous layers (Fig. 7b)

These intrafolial folds are typically asymmetric, tight to isoclinal single anticline-syncline fold pairs developed in a thin layer sandwiched between non-folded continuous layers (Fig. 7b). The fold axial planes lie at a low angle or parallel to the layers above and below. The hinges and limbs are relatively complete and intact. This type of F_1 fold is developed in lithological layers and in veins or sills parallel to the layers (Fig. 11b). Folds like these are often interpreted as "drag" folds produced by shear parallel to layering (mechanism 1 noted above). Ez (2000) questioned this model on the grounds that folds will form during shear only if the layers lie oblique to the deformation flow lines. However, most of the F_1 folds of this style showed no obvious relations to boudins or other embedded objects in the layering that produce initial deflections of layers oblique to the shearing direction.

Another proposed shear-related origin for such folds is that an initially upright fold became inclined due to layer-parallel shear, and simultaneously amplified and tightened by continuation of that shear strain (Skjernaa, 1980). Ez (2000) rejected this model because it required the folded layer to be competent (when it buckled) and passive (as it amplified) in the same deformation.

The flattening mechanism 2 explains these folds best as shown in Fig. 11a. The fold will tighten with increasing layer-normal shortening if it was initially overturned, otherwise the interlimb angle will progressively increase until the fold is unfolded (Fig. 11a). An intrafolial fold will form, as shown, in those layers that were initially
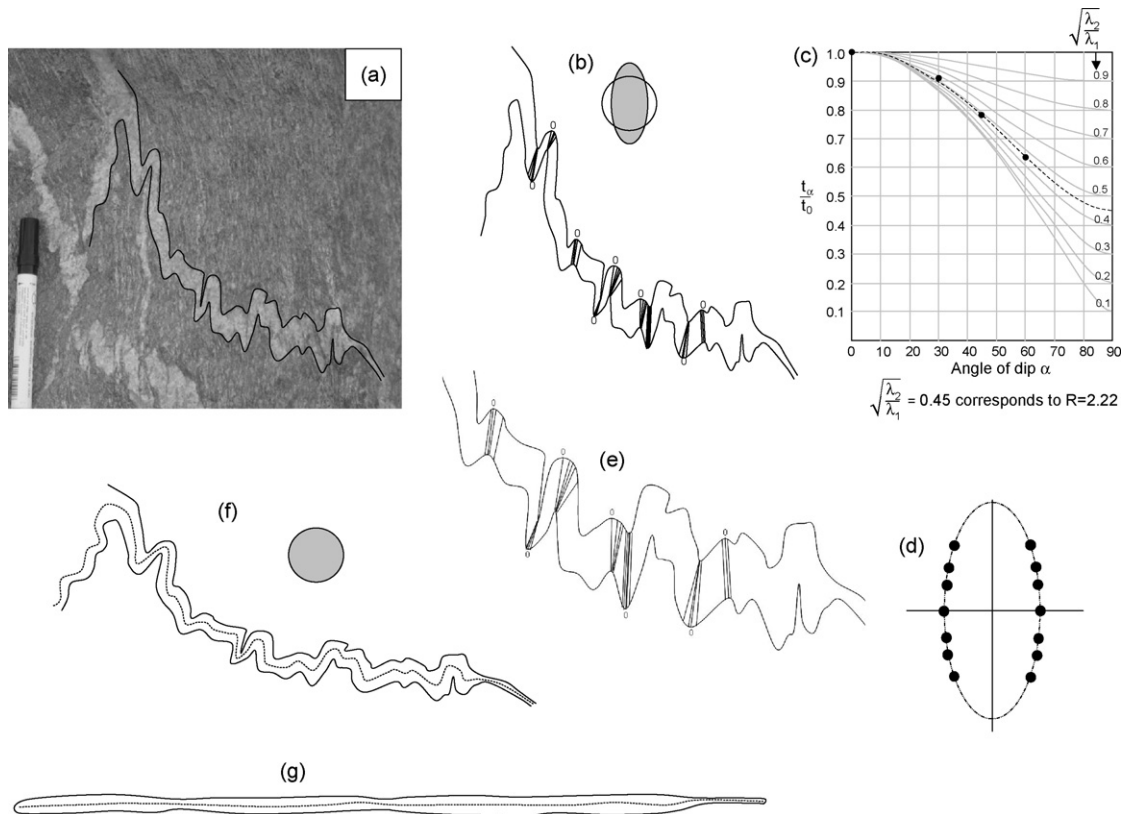
Fig. 12. Minimum layer-normal shortening strain estimates based on F_1 folds. (a) Example of F_1 fold developed in granitoid dykelet (Wadi Feiran). The folds are viewed looking along the hinge so this is an approximate YZ section. (b) Dip isogons for the folded layer shown in (a). Also strain R_{YZ} ellipse for these folds using Ramsay's (1967, p. 413) method for estimating strain which assumes the folds were originally type 1B style, and have attained their present style by superimposed bulk homogeneous flattening. (c) Graphic estimation of strain for the folds in (a) using Ramsay's method gives $R_{YZ} = 2.22$. (d) Estimation of strain for the folds in (a) using Lisle's (1992) method gives $R_{YZ} = 2.24$. (e) Details of the dip isogons for the folds in (a). (f) Restorations of the folds in (a) by unstraining to show the fold style before layer-normal homogeneous flattening. Dotted line is the median surface of folds used to estimate buckle shortening of the dyke at -36%. (g) Removing the buckle shortening restores the folds in (f) to the original unfolded length. Combination of buckle shortening and homogeneous flattening gives total shortening in the Z direction of -57% since the intrusion of the dyke.

overturned. The regular layers above and below the fold are actually unfolded by de-amplification of the same fold. Intrafolial folds produced by this flattening mechanism commonly have thickened short overturned limbs, whereas those produced by layer-parallel shearing have thinned short overturned limbs (Weijermars, 1993; Ez, 2000) (Fig. 11c). The Feiran–Solaf F_1 folds show some thickening of their short overturned limbs consistent with a mechanism 2 origin. If the initial fold had a vertical limb, continued bulk layer-normal shortening may buckle this limb to produce subsidiary folds as shown in Fig. 11d and e.

### 4.4.3. Third style: F_1 folds truncated by S_1 foliation (Fig. 7c)

Fold of this style are idealized in the sketch shown in Fig. 7c, and an example of this style is shown in Fig. 11j. Close inspection of these folds reveals that they can be traced into folds with one limb highly shear strained. Thus some have similarities to extensional crenulations (ECCs) where back-rotation of slices of foliation occurs between close-spaced extensional shear bands (Platt and Vissers, 1980). The difference between ECCs and this type of F_1 fold lies in the greater degree of F_1 folding of the foliation between the shear bands and the lower angle between the shear bands and the surrounding foliation. Harris (2003) shows very similar examples of cm-spaced ductile extensional shears in gneisses with tightly folded foliation between the shears. Harris et al. (2002) explain that these folds form by shortening of foliation between the shears as the foliation is back-rotated into the shortening field (Fig. 11h). The shears themselves rotate towards the flattening plane and are commonly intruded by pegmatite. This is probably the origin of the fold shown in Fig. 13a. The style of this fold is close to class 1B (Fig. 13b) and the strain ellipse related to S_1-normal flattening and L_1-parallel stretching of the fold is estimated by the method of Ramsay (1967) to have $R_{YZ} \sim 9.1$ (Fig. 13c). Another example of this style of F_1 folds is shown in Fig. 11i where the back-rotation has occurred during development of internal boudins.

The back-rotational axis involved in this mechanism lies parallel to X since the displacement on the ductile shears is controlled by Y. This again results in the F_1 folds having hinges parallel to the L_1 stretching lineation.

4.4.4. Significance of F_1 fold asymmetries – no regional D1 shearing – no F_1 macrofolds

Each of the styles of F_1 folds has its own history of initiation and amplification. The significance of the F_1 fold asymmetries also varies according to type. The asymmetry of F_1 folds produced by flattening of discordant dykes and veins reflects their original angular relations to S_1. The asymmetry of F_1 folds in continuous layers is the same as that of the original overturned fold from which it formed. The asymmetry of the shear truncated F_1 folds is controlled by the back-rotation sense on the shears. A shear and its conjugate will have opposite senses of back-rotation, and so the F_1 folds associated with each will have opposite senses of asymmetry (Harris, 2003). In fact there is no consistent F_1 fold asymmetry pattern in the Feiran gneisses (Fig. 14), and therefore claims that either the F_1 folds are drag folds indicating the vergence of a D1 regional thrusting event or are parasitic on the limbs of macroscopic F_1 folds (Hegazi, 1988; El-Shafei and Kusky, 2003; Sultan, 2003) are not supported by the data.
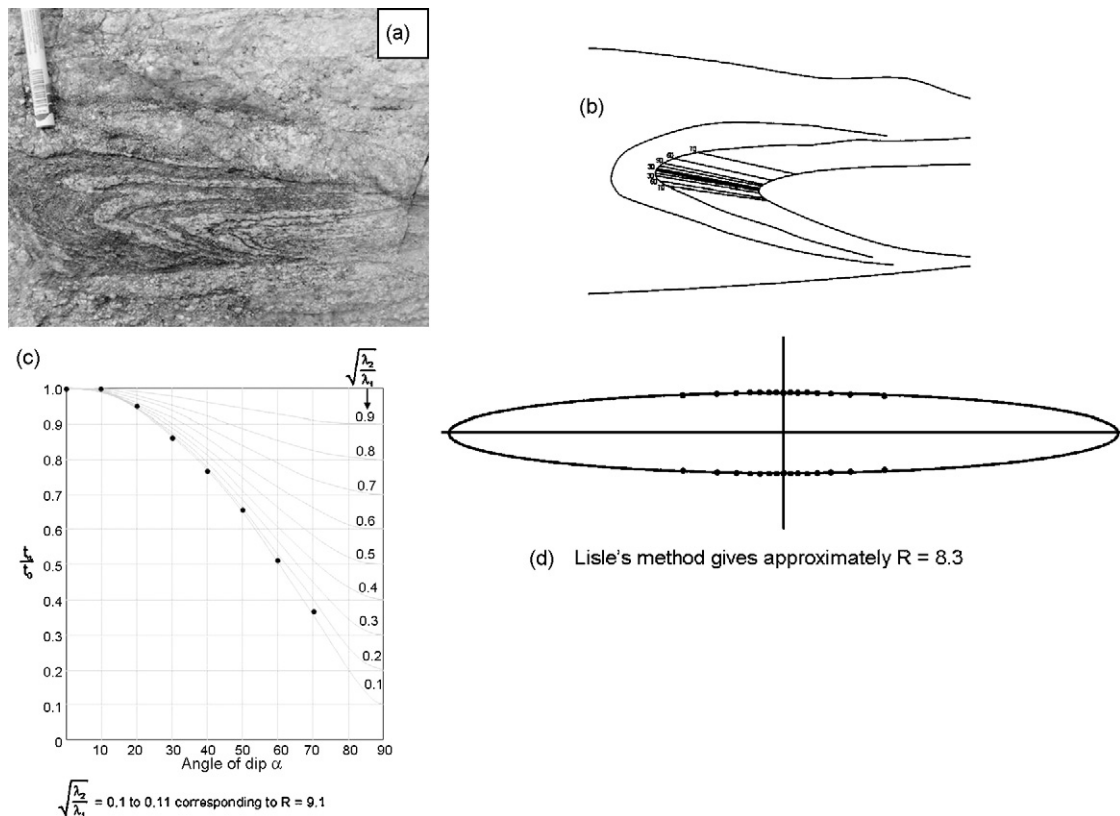
Fig. 13. Minimum layer-normal shortening strain estimates based on F_1 folds. (a) Example of F_1 folded S_1 foliation bounded above and below by granitoid intruded shears (Wadi Agala). View of the fold is along the hinge, i.e. along L_1 (parallel to X), so the plane of the fold is approximately the YZ plane of the finite strain ellipsoid. (b) Dip isogons for the fold in (a). (c) Graphic estimation of strain for the folds in (a) using Ramsay's method gives $R_{YZ} = 9.1$. (d) Estimation of strain for the folds in (a) using Lisle's (1992) method gives $R_{YZ} = 8.3$. After unstraining the fold changes interlimb angle from 22° to 108° so that the amount of buckle shortening is small at about −15%.

4.5. Summary so far

The above data have shown that the S_1 gneissic foliation (and the high temperature metamorphic event that produced it) and the F_1 intrafolial folds were all formed in a progressive coaxial approximately layer-normal flattening strain regime with no evidence for bulk/regional layer-parallel shearing. The next folding event (F_2) has the characteristics of layer-parallel (or approximately so) shortening and relations to compressional shearing at lower temperatures. This indicates that F_1 and F_2 are quite separate kinematically at least, and cannot be grouped in a single high temperature deformation event (Table 1) characterized by NE-SW shortening as suggested by El-Shafei and Kusky (2003). In the discussion below we consider the tectonic setting of S_1 and F_1.

5. Discussion

5.1. Unfolding the layers to original horizontal yields NNW-SSE trending L_1

S_1 and S_0 are macroscopically folded about gently SE plunging axes (Fig. 5). The macroscopic folds responsible are evidently the Feiran and Solaf antiforms (Fig. 2). We are particularly interested to see what pattern of L_1 lineations results from unfolding these antiforms. The existing map pattern of L_1 lineations is shown in Fig. 15a, where it is clear that the L_1 lineations on the NE limb of the Solaf Antiform plunge N to NW. The L_1 lineations in the hinge zone, and on the SW limb of the Solaf Antiform, plunge S to SE. The boundary between these L_1 orientation domains is not the approximate axial plane of the Solaf Antiform but does mark the boundary between its broad hinge zone and the NE limb. The

relationships between average foliation dip and L_1 orientation is shown in Fig. 15b. Restoring the foliations to horizontal yields an approximately constant NNW-SSE orientation for L_1. The relationship between L_1 plunge and position on the Feiran Antiform is not quite as clear since data for the northern limb is scarce. However the L_1 lineations reverse their direction of plunge from the northern limb to the southern limb in a similar manner to that for the Solaf Antiform. The restored L_1 lineations have a more northwesterly trend. It is not clear whether the difference between the Feiran and Solaf calculated original L_1 orientations is real or due to some rotation following folding. Nevertheless the results suggest that the original L_1 orientation, and hence regional extensional direction, was NNW-SSE to NW-SE.

5.2. The Feiran–Solaf gneissification was an extensional tectonic event

The deformation regime (D1) during gneissification and migmatization of the Feiran–Solaf metasediments was characterized by high temperature–low pressure metamorphism (maximum depth 15 km), vertical shortening (Z direction), horizontal extension in both the X and Y directions, and no evidence for macrofolding or regional shear parallel to the lithological layers. These are the characteristics of an extensional tectonic setting. Eliwa et al. (2004) also argued for an extensional tectonic setting of the Feiran–Solaf gneisses on the basis of the low P–high T characteristics of the metamorphism. Other features of the terrain that may constrain the extensional environment are (1) the gneiss protoliths were metasediments that consisted dominantly of quartz-rich psammites, pelites and calcareous pelites (El-Gaby and Ahmed, 1980; Shimron, 1984, 1988; Hassan and Hashad, 1990), though very minor
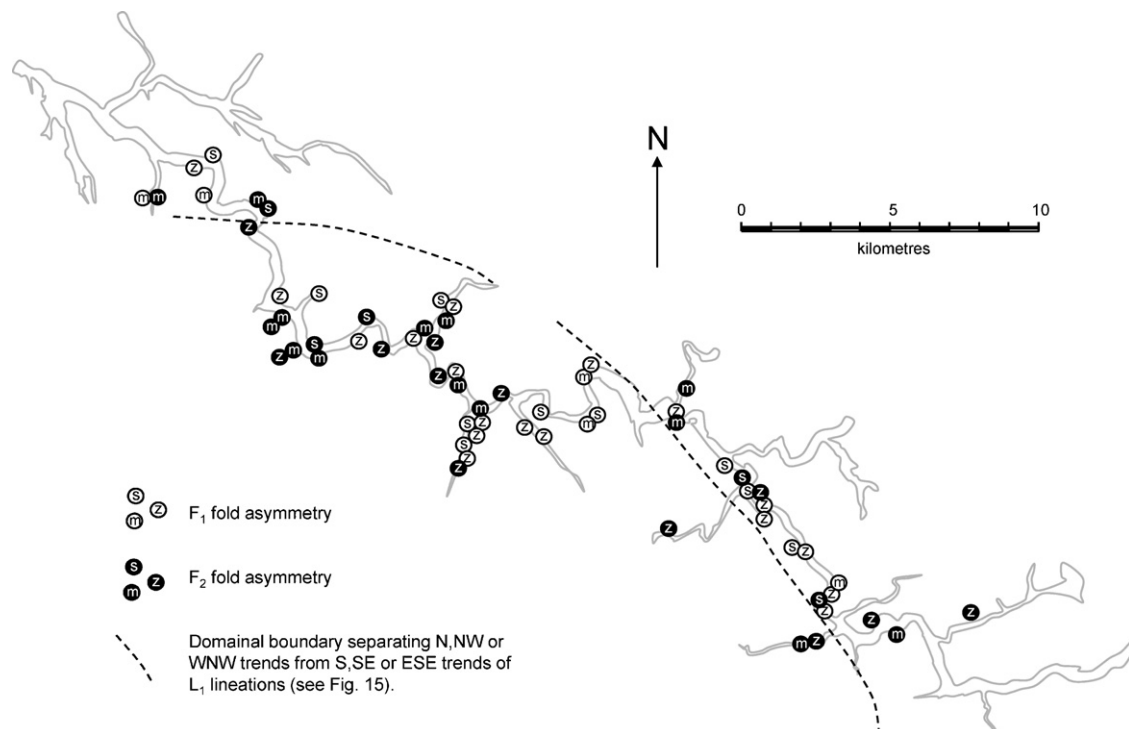
Fig. 14. Mapped distribution of F_1 and F_2 fold asymmetries expressed as m-, s-, and z-folds. There are no clear domains for F_1 asymmetry types and therefore no evidence for macroscopic F_1 folds can be based on this data. The dotted lines separate orientation domains for L_1 plunges (see Fig. 15) so that north and NE of these two dotted lines the L_1 lineations are NW (or N or WNW) plunging; while south and SW of these dotted lines the L_1 lineations are SE (or S or ESE) plunging. The reason for including these lines on this map of fold asymmetries is that F_1 and F_2 fold hinges are parallel to L_1. Since L_1 lineations show later fold-related reversals of plunge, so will F_1 (and F_2) hinges. Reversing the plunge of an F_1 asymmetric fold will turn s-folds into z-folds and vice versa. Taking this into account (by searching for patterns on one side of the dotted lines, then the other) still does not reveal any F_1 asymmetry domains.
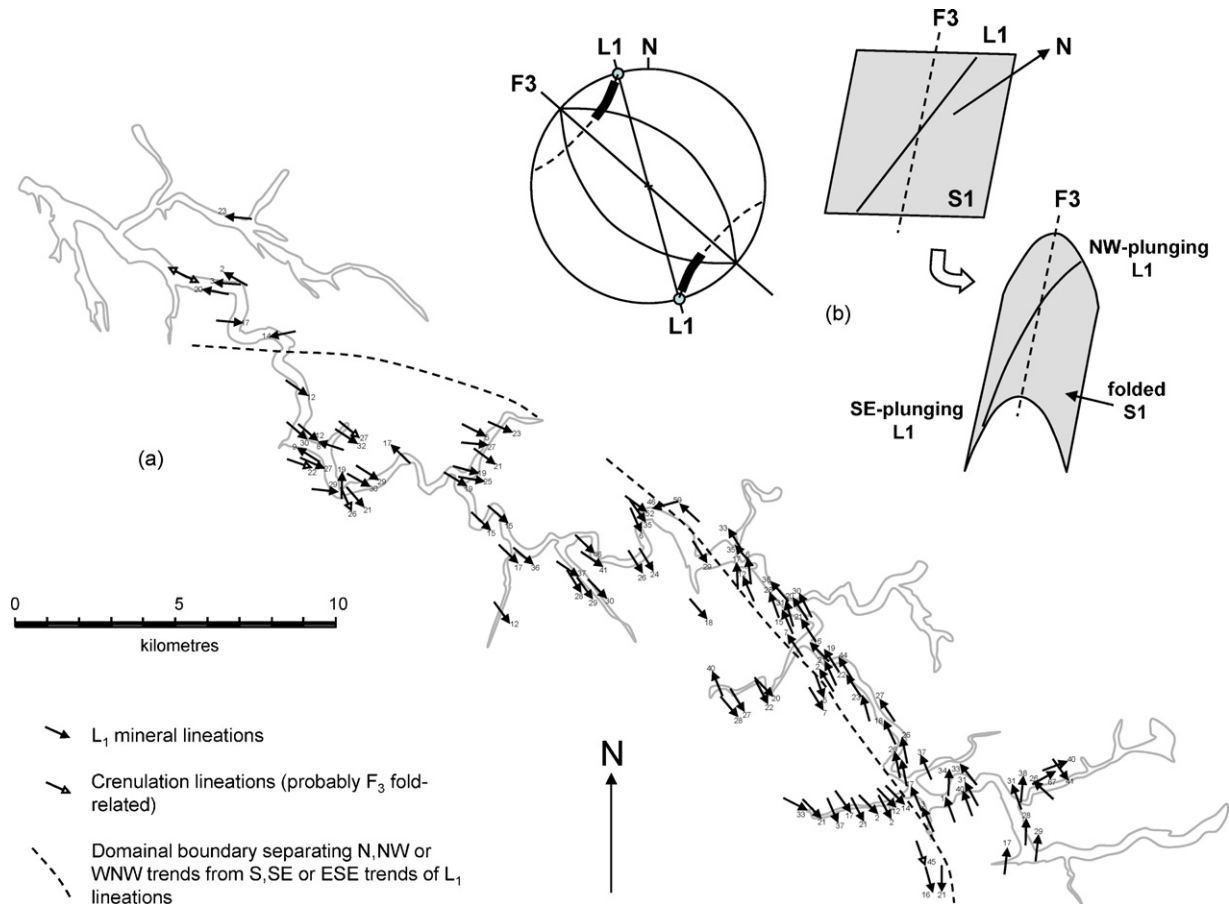
Fig. 15. Explanation of the tendency for L_1 lineations to pitch to the SE on S_1 foliations in Wadi Feiran, but pitch to the NW on S_1 foliations in Wadi Solaf. (a) Map of L_1 lineation orientations. The dotted lines separate NW (N or WNW) plunging L_1 lineations lying N and NE of the dotted lines, from SE (S or ESE) plunging L_1 lineations lying S and SW of the dotted lines. The dotted line in Wadi Feiran approximately follows the Feiran antiformal trace. The dotted line in Wadi Solaf is parallel to the trace of the Solaf antiform but lies rather at the junction of the NE dipping limb and the broad gently dipping hinge zone of this antiform. (b) The sketches explain the patterns seen in (a) as folding of L_1 (and S_1) by the F_3 Feiran and Solaf antiforms. The stereogram shows how the L_1 lineations have acquired NW and SE plunges. The reason for SE pitching L_1 on most Feiran S_1 foliations is because Wadi Feiran meanders mainly through the SW-dipping limb of the Feiran antiform. The NW pitch of L_1 lineations on most Solaf S_1 foliations is due to Wadi Solaf meandering through the NE dipping limb.

volcanic contribution was suggested by El Tokhi (2003), and Stern and Manton (1987, 1988) argued that the Feiran Group at least may have a volcanigenic component. (2) A high geothermal gradient of about $50\,^{\circ}\mathrm{C\,km^{-1}}$ is required to raise temperatures to $700 \pm 50\,^{\circ}\mathrm{C}$ at these depths. (3) There are abundant sills of dioritic, tonalitic and granodioritic composition that intruded syn-D1.

The basinal setting for the Feiran–Solaf sequence has been suggested to be a shallow-water platform, or perhaps a continental slope not far from the land mass (Shimron, 1980, 1984). Deposition of the mainly non-volcanigenic sequence occurred before the magmatic arc stage (Shimron, 1988) that produced the protoliths of the Elat gneissic terrain to the east at 810–780 Ma (Halpern and Tristan, 1981; Bielski, 1982; Kröner et al., 1990; Eyal et al., 1992; Abu El-Enen et al., 2003). These data argue against a back-arc, fore-arc or inter-arc basin setting and favour a pre-800 Ma intracontinental or continental margin depositional environment, perhaps a result of the initial rifting of Rodinia (Stern, 1994).

The abundant syn-D1 gneissic diorite, tonalite and granodiorite sills semi-concordantly *within* the Feiran gneisses probably also played a role in heat transfer during the high temperature metamorphism. Melts of this composition in the Arabian Nubian Shield are generally considered to be subduction-related. Hooper et al. (1995) challenged this assumption and argued that decompression melting of the subcontinental lithosphere is also a mechanism for

this magmatism. Recent studies by Xu et al. (2002) and Wang et al. (2006) have also indicated that these magmas may form by partial melting of delaminated lower crust by hot rising asthenosphere in extensional terrains.

Other tectonic events yielding terrains with sub-horizontal high temperature foliations and having pronounced extensional character include (1) *gravitational collapse* (Dewey, 1988, Rey et al., 2001); (2) *low-angle ductile normal shear-sense detachment zones* (Holcombe et al., 1991); (3) *metamorphic core complexes* (Crittenden et al., 1980; Coney and Harms, 1984; Lister and Davis, 1989; Roberts and Yielding, 1994); and (4) *mantled gneiss domes* (Holm and Lux, 1996; Teyssier and Whitney, 2002).

Gravitational collapse usually follows or accompanies crustal thickening associated with compressional orogeny (Fowler and El-Kalioubi, 2004; Kirkland et al., 2006), and we have no evidence for such an event. Low-angle normal-sense detachment zone produces decollement and pervasive ductile shearing which are not evident at the present exposure level, but may affect the basement underlying the Feiran gneisses. Metamorphic core complex comprises an older metamorphic-plutonic basement overlain by a foliated and lineated mylonitic or gneissic carapace separating the high grade metamorphic rocks below from low-grade or unmetamorphosed cover. Intermediate metamorphic levels are excised by successive splays of the detachment fault. There are no metamorphic grade

contrasts of this nature in the Feiran gneisses and no mylonitic carapace. Mantled gneiss domes are associated with diapiric rise of lower-density migmatitic rocks or plutons that updome the high temperature gneisses and schists overlying them (Lee et al., 2004). The strain patterns of these structures are quite complexly variable from intensely constrictional to pure flattening. Foliations and lineations likewise show complex orientation patterns. These are not characteristics of the Feiran–Solaf terrain.

Thus the continental rifting tectonic setting for the Feiran–Solaf D1 event appears to be the best model based on the available evidence and is the model preferred in this study.

6. Summary and conclusions

The gneissic and migmatitic rocks of the Feiran–Solaf belt in SW Sinai have mainly metasedimentary origin, with lesser synmetamorphic sills of gneissic diorite, tonalite, granodiorite and granite. The gneissosity is typically parallel to lithological layering S_0. A strong rod-like mineral lineation L_1 represents the stretching direction on S_1. The event during which S_1 and L_1 formed is termed D1. Another D1 structure is chocolate tablet boudinage and equivalent lensoidal pinch-and-swell structures. Minimum strain estimates based on the boudins indicate considerable shortening normal to S_1 (the Z principal strain direction) and significant extension in S_1 in both the X and Y directions. Tight to isoclinal intrafolial F_1 folds also formed during D1 and are related to continuing shortening normal to S_1 combined with dyking and veining across S_1 and back-rotation of S_1 and lithological layers on D1 extensional ductile shears. Strong L_1 development has produced in-plane plastic anisotropy in S_1 so that syn-S_1 dykes, veins and extensional shears lie parallel to L_1. This resulted in F_1 hinges also lying parallel to L_1.

Earlier studies of the Feiran–Solaf folds lacked clear criteria for distinguishing F_1 folds from later F_2 folds resulting in confusion about F_1 asymmetry patterns and deformation regime. We find that F_1 mesoscopic fold asymmetries do not indicate the presence of F_1 macrofolds, and are not a result of foliation-parallel shearing. Syn-gneissosity folds (F_1) should not be grouped with later tight "similar" F_2 folds which are probably thrust related but post-date the gneissosity. The D1 gneissosity-forming and migmatization event was an extensional tectonic event involving sustained vertical shortening and horizontal extension of lithological layers before the layers had experienced any significant folding. The tectonic environment for D1 is believed to have been a pre-800 Ma actively extending intracratonic rift that characterized an early stage of the break-up of Rodinia.

Acknowledgements

References

Abdel-Meguid, A.A., 1992. Late Proterozoic Pan African tectonic evolution of the Egyptian part of the Arabian-Nubian Shield. M. E. R. C. Ain Shams Univ. 6, 13–28.

Abu El-Enen, M.M., Okrusch, M., Will, T.M., 2003. The metamorphic evolution of the Pan-African basement in the Sinai Peninsula Egypt. In: Proceedings of the 5th International Conference on Geology of the Middle East, Cairo, Egypt, pp. 207–217.

Ahmed, A.A., 1970. Geology of the Area Around Feiran Oasis, Sinai. Ph.D. Thesis. Assiut Univ., Egypt.

Ahmed, A.A., 1981. Reconsidered view on Feiran–Solaf Gneisses southwest of Sinai, Egypt. Bull. Fac. Sci. Assiut Univ. 10, 131–142.

Akaad, M.K., 1959. The migmatitic gneisses of Wadi Feiran, Sinai, Egypt. Assiut Bull. Sci. Tech. II, 211–237.

Akaad, M.K., El-Gaby, S., Abbas, A.A., 1967a. Geology and petrography of the migmatites around Feiran Oasis, Sinai. Assiut Sci. Tech. Bull. 10, 67–87.

Akaad, M.K., El-Gaby, S., Abbas, A.A., 1967b. On the evolution of Feiran migmatites, Sinai. J. Geol. U.A.R. 11, 49–58.

Ball, J., 1916. Geography and geology of West Central Sinai. Egypt Survey Department, Cairo, 219 pp.

Barron, T., 1907. The topography and geology of the Peninsula of Sinai (Western portion). Egypt Survey Department, Cairo, 241 pp.

Belasy, M.R., 1991. Geology, petrography, and geochemistry of the metamorphic rocks of Wadi Feiran–Solaf area, southwestern Sinai, Egypt. Ph.D. Thesis. Faculty of Science, Zagazig Univ., 386 pp.

Bielski, M., 1982. Stages in the evolution of the Arabian-Nubian massif in Sinai, Egypt. PhD Thesis. Hebrew University, Jerusalem, 155 pp.

Canova, G., Kocks, U.F., Tome, C.N., Jonas, J.J., 1985. The yield surface of textured polycrystals. J. Mech. Phys. Solids 33, 371–397.

Coney, P.J., Harms, T.A., 1984. Cordilleran metamorphic core complexes: Cenozoic extensional relics of Mesozoic compression. Geology 12, 550–554.

Crittenden, M.D., Coney, P.J., Davis, G.H., 1980. Cordilleran metamorphic core complexes. Geol. Soc. Am. Mem. 153, 490.

Davis, G.H., 1984. Structural Geology of Rocks and Regions. Wiley, New York, 492 pp.

Dewey, J.F., 1988. Extensional collapse of orogens. Tectonics 7, 1123–1139.

El-Gaby, S., 1967. The mode of formation of cordierite gneisses in migmatitic rocks. Assiut Sci. Tech. Bull. 10, 91–106.

El-Gaby, S., Ahmed, A.A., 1980. The Feiran–Solaf gneiss belt, S.W. of Sinai, Egypt. I.A.G. Bulletin No. 3 "Evolution and Mineralization of the Arabian-Nubian Shield". Fac. Earth Sci., King Abdulaziz Univ. Jeddah. Pergamon Press. Oxford, pp. 95–105.

Eliwa, H.A., Abu El-Enen, M.M., Khalaf, I.M., Itaya, T., 2004. Metamorphic evolution of Sinai metapelites and gneisses: constraints from petrology and K/Ar dating. Egypt. J. Geol. 48, 169–185.

El-Shafei, M.K., 1998. Structural evolution of Feiran–Solaf metamorphic belt, SW Sinai, Egypt. Ph.D. Thesis. Suez Canal Univ., Ismailia, Egypt, 172 pp.

El-Shafei, M.K., Kusky, T.M., 2003. Structural and tectonic evolution of the Neoproterozoic Feiran–Solaf metamorphic belt Sinai Peninsula: implications for the closure of the Mozambique Ocean. Precam. Res. 123, 269–293.

El Tokhi, M., 1990. Petrographical, geochemical and experimental studies on the Migmatite Rocks of Wadi Feiran, Southern Sinai, Egypt. Ph.D. Thesis. El-Mansoura University, Egypt, 98 pp.

El Tokhi, M.M., 1992. Origin and tectonic implications of Pan-African amphibolites of Wadi Feiran South Sinai. In: Proceedings of the third conference on Geology of Sinai Development, Ismailia, pp. 239–248.

El Tokhi, M.M., 2003. Petrogenesis, geochemistry and origin of the Precambrian gneisses of Feiran Complex, south western Sinai. Egypt. Ann. Geol. Surv. XXVI, 1–17.

Eyal, Y., Eyal, M., Kröner, A., 1992. Geochronology of the Elat Terrain, metamorphic basement, and its implications for crustal evolution of the NE part of the Arabian-Nubian Shield. Isr. J. Earth Sci. 40, 5–16.

Ez, V., 2000. When shearing is a cause of folding. Earth Sci. Rev. 51, 155–172.

Fowler, A., El-Kalioubi, B., 2004. Gravitational collapse origin of shear zones, foliations and linear structures in the Neoproterozoic cover nappes, Eastern Desert. Egypt. J. Afr. Earth Sci. 38, 23–40.

Ghosh, S.K., 1988. Theory of chocolate tablet boudinage. J. Struct. Geol. 10, 541–553.

Ghosh, S.K., 1993. Structural Geology. Fundamentals and Modern Developments. Pergamon Press, New York, 598 pp.

Gottschalk, R.R., Kronenberg, A.K., Russell, J.E., Handin, J., 1990. Mechanical anisotropy of gneiss: failure criterion and textural sources of directional behaviour. J. Geophys. Res. 95, 21613–21634.

Halpern, M., Tristan, N., 1981. Geochronology of the Arabian-Nubian Shield in southern Israel and eastern Sinai. J. Geol. 89, 639–648.

Harris, L.B., 2003. Folding in high-grade rocks due to back-rotation between shear zones. J. Struct. Geol. 25, 223–240.

Harris, L.B., Koyi, H.A., Fossen, H., 2002. Mechanisms for folding of high-grade rocks in extensional tectonic settings. Earth Sci. Rev. 59, 163–210.

Hashad, M.H., Hassen, I.S., El Kalioubi, B., 2001. Petrology and mineralogy of calc-silicate gneisses and their significance as indicators of metamorphism in southeastern Sinai. Egypt. Mineral. 13, 187–223.

Hassan, M.A., Hashad, A.H., 1990. Precambrian of Egypt. In: Said, R. (Ed.), The Geology of Egypt. Balkema, Rotterdam, pp. 201–245.

Hatcher, R.D., 1995. Structural Geology. Principles, Concepts and Problems, 2nd ed. Prentice-Hall, New Jersey, 525 pp.

Hegazi, A.M., 1988. Structural studies on the Feiran Oasis area, central Sinai, Egypt. M.Sc. Thesis. Suez Canal Univ., Ismailia, Egypt, 81 pp.

Hegazi, A.M., El-Shafei, M.K., Sultan, Y.M., 2004. Multiple deformation phases of Solaf Gneiss Belt, South Sinai Egypt. In: Proceedings of the 7th International Conference on Geology of the Arab World, Cairo, pp. 313–320.

Hobbs, B.E., Means, W.D., Williams, P.F., 1976. An Outline of Structural Geology. Wiley, New York, 571 pp.

　　　　　　　　　　　　　　　　　　A. Fowler, I. Hassan / Precambrian Research 164 (2008) 119–136

Holcombe, R.J., Pearson, P.J., Oliver, N.H.S., 1991. Geometry of a Middle Protero-zoic extensional décollement in northeastern Australia. Tectonophysics 191, 255–274.

Holm, D.K., Lux, D.R., 1996. Core complex model proposed for gneiss dome devel-opment during collapse of the Paleoproterozoic Penokean orogen, Minnesota. Geology 24, 343–346.

Hooper, P.R., Bailey, D.G., McCarley Holder, G.A., 1995. Tertiary calc-alkaline magma-tism associated with lithospheric extension in the Pacific Northwest. J. Geophys. Res. 100, 10303–10319.

Hosford, W.F., 1998. Reflections on the dependence of plastic anisotropy on texture. Mater. Sci. Eng. A 257, 1–8.

Hume, W.F., 1906. The topography and geology of the Peninsula of Sinai (Southeast-ern portion). Geological Survey of Egypt, Cairo, 280 pp.

Hume, W.F., 1934. Geology of Egypt. The Metamorphic Rocks, vol. 2. Geological Survey of Egypt, Cairo, Part 1, 300 pp.

Kabesh, M.L., 1993. Geological, petrological and geochemical studies on the migmatitic rocks of Wadi Feiran, south western Sinai, Egypt. Ph.D. Thesis. Cairo University, 183 pp.

Khawasik, S.M., 1995. Structural exploration of the green marble bed of Wadi Solaf South Sinai. In: Proceedings of the 4th Conference on Geology of Sinai Develop-ment, Ismailia, Egypt, pp. 13–25.

Kidan, T.W., Cosgrove, J.W., 1996. The deformation of multilayers by layer-normal compression; an experimental investigation. J. Struct. Geol. 18, 461–474.

Kirkland, C.L., Daly, J.S., Eide, E.A., Whitehouse, M.J., 2006. The structure and timing of lateral escape during the Scandian Orogeny: a combined strain and geochrono-logical investigation in Finnmark Arctic Norwegian Caledonides. Tectonophysics 425, 159–189.

Kröner, A., Eyal, M., Eyal, Y., 1990. Early Pan-African evolution of the basement around Elat, Israel, and the Sinai Peninsula revealed by single zircon evaporation dating, and implication of crustal accretion rates. Geology 18, 545–548.

Lacassin, R., Van Den Driessche, J., 1983. Finite strain determination of gneiss: appli-cation of Fry's method to porphyroid in the southern Massif Central (France). J. Struct. Geol. 5, 245–253.

Lee, J., Hacker, B., Wang, Y., 2004. Evolution of North Himalayan gneiss domes: struc-tural and metamorphic studies in Mabja Dome, southern Tibet. J. Struct. Geol. 26, 2297–2316.

Lisle, R.J., 1992. Strain estimation from flattened buckle folds. J. Struct. Geol. 14, 369–371.

Lister, G.S., Davis, G.A., 1989. The origin of metamorphic core complexes and detachment faults formed during Tertiary continental extension in the northern Colorado River region, U.S.A. J. Struct. Geol. 11, 65–94.

Man, C., 2002. On the r-value of textured sheet metals. Int. J. Plasticity 18, 1683–1706.

Means, W.D., 1989. Stretching faults. Geology 17, 893–896.

Mulchrone, K.F., 2002. A statistic for estimating strain with confidence intervals from deformed line distributions with an application to schists and gneisses of the Western Gneiss Region, west central Norway. J. Struct. Geol. 24, 545–556.

Odling, N.E., 1984. Strain analysis and strain path modelling in the Loch Tollie gneisses, Gairloch NW Scotland. J. Struct. Geol. 6, 543–562.

Park, R.G., 1997. Foundations of Structural Geology, 3rd ed. Routledge, London, 202 pp.

Passchier, C.W., 1998. Monoclinic model shear zones. J. Struct. Geol. 20, 1121–1137.

Platt, J.P., Vissers, R.L.M., 1980. Extensional structures in anisotropic rocks. J. Struct. Geol. 2, 397–410.

Poirier, J.P., 1980. Shear localization and shear instability in materials in the ductile field. J. Struct. Geol. 2, 135–142.

Price, N.J., Cosgrove, J.W., 1990. Analysis of Geological Structures. Cambridge Uni-versity Press, Cambridge, 502 pp.

Ramsay, J.G., 1967. Folding and Fracturing of Rocks. McGraw-Hill, New York, 568 pp.

Ramsay, J.G., Huber, M.I., 1983. The Techniques of Modern Structural Geology: Strain Analysis, vol. 1. Academic Press, London, 307 pp.

Rey, P., Vanderhaeghe, O., Teyssier, C., 2001. Gravitational collapse of the continental crust: definition, regimes and modes. Tectonophysics 342, 435–449.

Roberts, A., Yielding, G., 1994. Continental extensional tectonics. In: Hancock, P.L. (Ed.), Continental Deformation. Pergamon Press, Oxford, pp. 223–250.

Schürmann, H.M.E., 1953. The pre-Cambrian of the Gulf of Suez area. Comptes Ren-dus Inter. Geol. Cong. Sect. 1, Fasc. 1, Alger.

Schürmann, H.M.E., 1966. The Precambrian along the Gulf of Suez and the Northern Part of the Red Sea. Brill, Leiden, 404 pp.

Shimron, A.E., 1980. Proterozoic island arc volcanism and sedimentation in Sinai. Precam. Res. 12, 437–458.

Shimron, A., 1984. Metamorphism and tectonics of a Pan-African terrain in south-eastern Sinai: a discussion. Precam. Res. 24, 173–188.

Shimron, A.E., 1988. Discussion on the age of Feiran basement rocks Sinai: impli-cations for late Precambrian crustal evolution in the northern Arabian-Nubian Shield. J. Geol. Soc. Lond. 145, 1033–1034.

Skjernaa, L., 1980. Rotation and deformation of randomly oriented planar and linear structures in progressive simple shear. J. Struct. Geol. 2, 101–109.

Skrotzki, W., Tamm, R., Oertel, C.G., Beckers, B., Brokmeier, H.G., Rybacki, E., 2001. Tex-ture induced plastic anisotropy of NiAl polycrystals. Mater. Sci. Eng. A 319–321, 364–367.

Soliman, M., Azaz, S.A., Sabet, A.A., Aly, M.M., Belasy, M.R., 1988. Geochemistry and genesis of the migmatites of Wadi Feiran–Solaf area, southwestern Sinai, Egypt. Bull. Fac. Sci., Zagazig Univ. 10, 248–282.

Soto, J.I., 1991. Strain analysis method using the maximum frequency of unimodal deformed orientation distributions: applications to gneissic rocks. J. Struct. Geol. 13, 329–335.

Stern, R.J., 1994. Arc assembly and continental collision in the Neoproterozoic East African Orogen: implications for the consolidation of Gondwanaland. Ann. Rev. Earth Planet. Sci. 22, 319–351.

Stern, R.J., Manton, W.I., 1987. Age of Feiran basement rocks Sinai: implications for late Precambrian crustal evolution in the northern Arabian-Nubian Shield. J. Geol. Soc. Lond. 144, 569–575.

Stern, R.J., Manton, W.I., 1988. Discussion on the age of Feiran basement rocks Sinai: implications for late Precambrian crustal evolution in the northern Arabian-Nubian Shield. J. Geol. Soc. Lond. 145, 1034–1035.

Sultan, Y.M., 2003. Structural studies on Wadi Feiran - Wadi El-Sheikh area, south Sinai, Egypt. M. Sc. Thesis. Suez Canal University, Ismailia, 144 pp.

Takeshita, T., 1989. Plastic anisotropy in textured mineral aggregates: theories and geological implications. In: Karato, S., Toriumi, M. (Eds.), Rheology of Solids and of the Earth. Oxford University Press, New York, pp. 237–283.

Teyssier, C., Whitney, D.L., 2002. Gneiss domes and orogeny. Geology 30, 1139–1142.

Wang, Q., Xu, J.-F., Jian, P., Bao, Z.-W., Zhao, Z.-H., Li, C.-F., Xiong, X.-L., Ma, J.-L., 2006. Petrogenesis of adakitic porphyries in an extensional tectonic setting, Dexing South China: implications for the genesis of porphyry copper mineralization. J. Petrol. 47, 119–144.

Weijermars, R., 1993. Progressive deformation of single layers under constantly ori-ented boundary stresses. J. Struct. Geol. 15, 911–922.

Wenk, H.-R., Van Houtte, P., 2004. Texture and anisotropy. Rep. Prog. Phys. 67, 1367–1428.

Xu, J.-F., Shinjo, R., Defant, M.J., Wang, Q., Rapp, R.P., 2002. Origin of Mesozoic adakitic intrusive rocks in the Ningzhen area of east China: partial melting of delaminated lower continental crust? Geology 30, 1111–1114.